EUROPEAN ORGANIZATION FOR NUCLEAR RESEARCH (CERN)

CERN-EP-2018-2329
2019/01/03

CMS-HIG-18-002

Measurements of the Higgs boson width and anomalous HVV couplings from on-shell and off-shell production in the four-lepton final state

The CMS Collaboration*

Abstract

Studies of on-shell and off-shell Higgs boson production in the four-lepton final state are presented, using data from the CMS experiment at the LHC that correspond to an integrated luminosity of 80.2 fb^{-1} at a center-of-mass energy of 13 TeV. Joint constraints are set on the Higgs boson total width and parameters that express its anomalous couplings to two electroweak vector bosons. These results are combined with those obtained from the data collected at center-of-mass energies of 7 and 8 TeV, corresponding to integrated luminosities of 5.1 and 19.7 fb^{-1}, respectively. Kinematic information from the decay particles and the associated jets are combined using matrix element techniques to identify the production mechanism and to increase sensitivity to the Higgs boson couplings in both production and decay. The constraints on anomalous HVV couplings are found to be consistent with the standard model expectation in both the on-shell and off-shell regions. Under the assumption of a coupling structure similar to that in the standard model, the Higgs boson width is constrained to be $3.2^{+2.8}_{-2.2}$ MeV while the expected constraint based on simulation is $4.1^{+5.0}_{-4.0}$ MeV. The constraints on the width remain similar with the inclusion of the tested anomalous HVV interactions.

Submitted to Physical Review D

*See Appendix A for the list of collaboration members

1 Introduction

The standard model (SM) of particle physics postulates the existence of a Higgs field responsible for the generation of the masses of fundamental particles. The excitation of this field is known as the Higgs boson (H) [1–7]. The observation of an H boson with a mass of around 125 GeV by the ATLAS and CMS Collaborations [8–10] is consistent with the expectations of the SM, but further tests of the properties of this particle, such as its width and the structure of its couplings to the known SM particles, are needed to determine its nature.

The CMS and ATLAS experiments have set constraints of $\Gamma_{\mathrm{H}} < 13$ MeV at 95% confidence level (CL) on the H boson total width [11–15] using the off-shell production method [16–18], which relies on the relative measurement of off-shell and on-shell production. The upper bound on Γ_{H} was set considering the gluon fusion and electroweak (EW) production mechanisms in the analysis. The precision on Γ_{H} from on-shell measurements of the width of the resonance peak alone is approximately 1 GeV [19–21], which is significantly worse than the result from the off-shell method. The constraint on the H boson lifetime is equivalent to a lower bound on the width and was derived from the flight distance in the CMS detector as $\Gamma_{\mathrm{H}} > 3.5 \times 10^{-9}$ MeV at 95% CL [13]. The SM expectation of the width of the H boson is around 4 MeV [22].

The CMS [13, 23–27] and ATLAS [28–33] experiments have set constraints on the spin-parity properties and anomalous couplings of the H boson, finding its quantum numbers to be consistent with $J^{PC} = 0^{++}$, but allowing small anomalous couplings to two EW gauge bosons (anomalous HVV couplings). Off-shell signal production may be enhanced in the presence of these anomalous HVV couplings [11, 13, 22, 34–36]. As a result, the measurement of Γ_{H} using the off-shell technique may be affected by these deviations of the H boson couplings from the SM expectations. An attempt to measure Γ_{H} using the off-shell technique while including anomalous HVV interactions has been made by the CMS experiment [13]. In that previous study, constraints are placed on Γ_{H} and the on-shell cross-section fraction $f_{\Lambda\mathrm{Q}}$ that expresses an anomalous coupling contribution sensitive to the invariant mass of the H boson, using a realistic treatment of interference between the H boson signal and the continuum background. Extending the application of the off-shell technique to a wider range of anomalous HVV contributions, studied previously using on-shell H boson production [27], is the goal of this paper.

The presented investigation on the H boson width targets both gluon fusion and EW production mechanisms and tests the effects of possible anomalous HVV couplings in either production or decay. Nevertheless, it still relies on the knowledge of coupling ratios between the off-shell and on-shell production, the dominance of the top quark loop in the gluon fusion production mechanism, and the absence of new particle contributions in the loop. A violation of the last assumption by itself would be a manifestation of physics beyond the SM (BSM), which may become evident if the measured width deviates from the SM expectation. The measured width may also deviate from the SM expectation if the H boson has new BSM decay channels or the known channels have non-SM rates. Therefore, the measurement of the width complements the search for H boson decay to invisible or undetected particles, and the measurement of the H boson couplings to the known SM particles.

The data sample used in this analysis corresponds to integrated luminosities of 35.9 fb^{-1} collected in 2016 and 41.5 fb^{-1} collected in 2017 during Run 2 of the CERN LHC at a center-of-mass energy of 13 TeV. These results are combined with results obtained earlier from the data collected at center-of-mass energies of 7 TeV (in 2011), 8 TeV (in 2012), and 13 TeV (in 2015), corresponding to integrated luminosities of 5.1, 19.7, and 2.7 fb^{-1}, respectively [25, 27]. The increase in either energy and integrated luminosity leads to substantial improvement in the

precision of the width measurement using the off-shell technique, either under the assumption of SM couplings or with BSM effects.

This analysis follows closely the general $H \to 4\ell$ (leptons ℓ = e or μ) selection and reconstruction documented in Ref. [21] using the data collected in 2016, and the on-shell study of anomalous HVV couplings with the combined 2015 and 2016 data set in Ref. [27]. Many of the technical details of the search for a scalar resonance $X \to ZZ$ at high mass in Run 2 data, documented in Ref. [37], are also shared in the analyses presented here. The rest of the paper is organized as follows. The phenomenology of anomalous HVV interactions is discussed in Section 2. The CMS detector, reconstruction techniques, and Monte Carlo (MC) simulation methods are introduced in Section 3. The addition of the 2017 data to that used in Refs. [21, 27], and the relevant differences in the detector and reconstruction techniques are also discussed in this section. The details of the analysis are discussed in Sections 4 and 5, and the results are presented in Section 6. We provide a summary of these results in Section 7.

2 Phenomenology of anomalous HVV interactions

The constraints on Γ_H are set using the off-shell production method, which considers the H boson production relationship between the on-shell ($105 < m_{4\ell} < 140\,\text{GeV}$) and off-shell ($m_{4\ell} > 220\,\text{GeV}$) regions. Denoting each production mechanism with $vv \to H \to VV \to 4\ell$ for the H boson coupling to either strong ($vv = gg$) or EW ($vv = WW, ZZ, Z\gamma, \gamma\gamma$) vector bosons in its production, the on-shell and off-shell H boson signal yields are related by [16]

$$\sigma^{\text{on-shell}}_{vv\to H\to 4\ell} \propto \mu_{vvH} \quad \text{and} \quad \sigma^{\text{off-shell}}_{vv\to H\to 4\ell} \propto \mu_{vvH}\,\Gamma_H, \tag{1}$$

where μ_{vvH} is defined as the on-shell signal strength, the ratio of the observed number of on-shell four-lepton events relative to the SM expectation. This ratio is interpreted as either μ_F for H boson production via gluon fusion (ggH) or in association with a $t\bar{t}$ ($t\bar{t}H$) or $b\bar{b}$ pair ($b\bar{b}H$), or μ_V for H boson production via vector boson fusion (VBF) or in association with an EW vector boson W or Z (VH). There is sizable interference between the H boson signal and the continuum background in the off-shell region [17], contrary to on-shell production, and this formalism scales the interference contribution with $\sqrt{\mu_{vvH}\,\Gamma_H}$.

This analysis is based on a phenomenological framework [22, 38–59] that describes the anomalous couplings of a Higgs-like boson to two gauge bosons, such as $WW, ZZ, Z\gamma, \gamma\gamma$, and gg. These couplings appear in either the production of the H boson or its decay, regardless of the $m_{4\ell}$ region in which the H boson is produced. The relationship in Eq. (1) is therefore meant to imply concurrent variations in vvH couplings in both on-shell and off-shell regions. The coupling of the H boson to two gluons is assumed to be as in the SM, via quark loops with Yukawa couplings to quarks, where the contribution from the top-quark is dominant. This assumption is valid as long as the production is dominated by the top-quark loop and no new particles contribute to this loop. The Yukawa couplings also appear in direct interactions with fermion-antifermion pairs, such as in $t\bar{t}H$ and $b\bar{b}H$ productions. These interactions are of less importance in this study, since they are highly suppressed at high off-shell mass, but they are included in the analysis of the on-shell H boson production with similar assumptions as in the case of production via gluon fusion. Variation of the HVV couplings, in either the VBF or VH productions, or the $H \to 4\ell$ decay, are allowed to depend on anomalous coupling contributions.

In the following, we assume that the H boson couples to two gauge bosons VV, such as WW, ZZ, $Z\gamma$ or $\gamma\gamma$, which in turn couple to fermions, either four leptons in H boson decay, or quarks

or leptons in its production or in the decay of associated EW bosons. It is assumed that the H boson does not couple to fermions through a new heavy state, generating a so-called contact interaction [57, 58]. However, the inclusion of amplitude terms pertaining to contact interactions is equivalent to the anomalous HVV couplings already tested [25] under the assumption of flavor universality in $\mathrm{V}\bar{\mathrm{f}}\mathrm{f}$ couplings. Both approaches test three general tensor structures allowed by Lorentz symmetry, with form factors $F_i(q_1^2, q_2^2)$ in front of each term, where q_1 and q_2 are the four-momenta of the two difermion states, such as $(\mathrm{e}^+\mathrm{e}^-)$ and $(\mu^+\mu^-)$ in the $\mathrm{H} \to \mathrm{e}^+\mathrm{e}^-\mu^+\mu^-$ decay, and equivalent states in production. We also fix all lepton and quark couplings to vector bosons according to SM expectations. Relaxing this requirement would make it equivalent to flavor nonuniversal couplings of the contact terms, but would also introduce too many unconstrained parameters, which cannot be tested with the present data sample. Only the lowest order operators, or lowest order terms in the (q_j^2/Λ^2) form-factor expansion, are tested, where Λ is the energy scale of new physics.

The signal scattering amplitude describing the interaction between a spin-zero H boson and two spin-one gauge bosons VV is written as [54]

$$A \sim \left[a_1^{\mathrm{VV}} - \frac{\kappa_1^{\mathrm{VV}} q_1^2 + \kappa_2^{\mathrm{VV}} q_2^2}{\left(\Lambda_1^{\mathrm{VV}}\right)^2} - \frac{\kappa_3^{\mathrm{VV}} (q_1+q_2)^2}{\left(\Lambda_{\mathrm{Q}}^{\mathrm{VV}}\right)^2} \right] m_{\mathrm{V1}}^2 \epsilon_{\mathrm{V1}}^* \epsilon_{\mathrm{V2}}^* + a_2^{\mathrm{VV}} f_{\mu\nu}^{*(1)} f^{*(2)\,\mu\nu} + a_3^{\mathrm{VV}} f_{\mu\nu}^{*(1)} \tilde{f}^{*(2)\,\mu\nu}. \tag{2}$$

In this expression of the scattering amplitude, ϵ_i is the polarization vector of gauge boson V_i, $f^{(i)\mu\nu} = \epsilon_i^\mu q_i^\nu - \epsilon_i^\nu q_i^\mu$ is a scalar tensor constructed from this polarization vector and the momentum of the gauge boson, and $\tilde{f}_{\mu\nu}^{(i)} = \frac{1}{2}\epsilon_{\mu\nu\rho\sigma} f^{(i)\,\rho\sigma}$ is the pseudoscalar tensor counterpart. When at least one of the gauge bosons V is massive, m_{V1} is the pole mass of that gauge boson. The scales of BSM physics are denoted with Λ_1 and Λ_Q, so a_i^{VV}, or $1/\Lambda_1$ and $1/\Lambda_Q$, become the coupling-strength modifiers of the relevant HVV amplitudes, where a_i^{VV} may in general be any complex number, and $\left|\kappa_{1,2,3}^{\mathrm{VV}}\right| = 0$ or 1 are complex numbers. Under the assumption that the couplings are constant and real, the above formulation is equivalent to an effective Lagrangian notation. Therefore, in this paper, the real coupling constants are tested. The above approach allows a sufficiently general test of the $\mathrm{H} \to 4\ell$ kinematics in decay and equivalent kinematics in production, as discussed below, including production and decay of virtual intermediate photons. If deviations from the SM are detected, a more detailed study of $F_i(q_1^2, q_2^2)$ could be performed, eventually providing a measurement of the double-differential cross section for each tensor structure tested.

In the above, the only leading tree-level contributions are $a_1^{\mathrm{ZZ}} \neq 0$ and $a_1^{\mathrm{WW}} \neq 0$, and in the following we assume the custodial symmetry $a_1^{\mathrm{ZZ}} = a_1^{\mathrm{WW}}$. The rest of the couplings are considered anomalous contributions, which are either tiny contributions arising in the SM due to loop effects or new BSM contributions. The SM loop contributions are not accessible experimentally with the available data. Among anomalous contributions, considerations of symmetry and gauge invariance require $\kappa_1^{\mathrm{ZZ}} = \kappa_2^{\mathrm{ZZ}} = -\exp(i\phi_{\Lambda 1}^{\mathrm{ZZ}})$, $\kappa_1^{\gamma\gamma} = \kappa_2^{\gamma\gamma} = 0$, $\kappa_1^{\mathrm{gg}} = \kappa_2^{\mathrm{gg}} = 0$, $\kappa_1^{\mathrm{Z}\gamma} = 0$, and $\kappa_2^{\mathrm{Z}\gamma} = -\exp(i\phi_{\Lambda 1}^{\mathrm{Z}\gamma})$. While not strictly required, the same symmetry is considered in the WW case $\kappa_1^{\mathrm{WW}} = \kappa_2^{\mathrm{WW}} = -\exp(i\phi_{\Lambda 1}^{\mathrm{WW}})$.

Neither $\mathrm{HZ}\gamma$ nor $\mathrm{H}\gamma\gamma$ couplings produce a sizable off-shell enhancement, since there is no interplay between the vector bosons or the H boson going off-shell, and there is no off-shell threshold for these couplings. Therefore, off-shell treatment for these couplings can be ignored. While the $a_{2,3}^{\mathrm{Z}\gamma}$ and $a_{2,3}^{\gamma\gamma}$ terms are tested in the Run 1 analysis [25], the precision of those constraints is still not competitive with the on-shell photon measurements in $\mathrm{H} \to \mathrm{Z}\gamma$ and $\gamma\gamma$. We,

therefore, omit those measurements in this paper. The Λ_Q term depends only on the invariant mass of the H boson, so its contribution is not distinguishable from the SM in the on-shell region and is only testable through the off-shell region. Tight constraints are already set on this parameter in the Run 1 analysis [13], so it is also not considered in this paper.

In the following, the ZZ labels for the ZZ interactions are omitted, and we use a generic notation a_i to denote a_3, a_2, $1/\Lambda_1$, and $1/\Lambda_1^{Z\gamma}$, which are the four couplings tested in this paper as listed in Table 1. Furthermore, the WW measurements are integrated into the ZZ measurements assuming $a_i^{ZZ} = a_i^{WW}$. The HWW contributions appear in the VBF and WH productions. This assumption does not affect the kinematic analysis of events because there is very little difference in kinematic distributions in events initiated by either WW or ZZ fusion. However, this assumption may affect the interpretation of the results should a different relationship between a_i^{ZZ} and a_i^{WW} be assumed. Therefore, such a scenario is discussed in more detail below by introducing the parameter r_{ai}, following Ref. [25], as

$$r_{ai} = \frac{a_i^{WW}/a_1^{WW}}{a_i/a_1}. \tag{3}$$

Including the parameter r_{ai} in the probability parameterization despite the lack of sensitivity of the data would introduce complexity without a comparable gain in physics content. We proceed with the analysis assuming $r_{ai} = 1$, but point out below how results could be reinterpreted should a different value be assumed.

Most systematic uncertainties cancel when taking ratios to the total cross section, so measurements of a_i relative to the dominant SM-like contribution a_1 are the preferred approach. For this purpose, the effective fractional ZZ cross sections f_{ai} and phases ϕ_{ai} are defined as

$$\begin{aligned} f_{ai} &= \frac{|a_i|^2\sigma_i}{\sum_{j=1,2,3\ldots}|a_j|^2\sigma_j}, \\ \phi_{ai} &= \arg\left(\frac{a_i}{a_1}\right), \end{aligned} \tag{4}$$

where σ_i is the cross section for the process corresponding to $a_i = 1$, $a_{j\neq i} = 0$, while $\tilde{\sigma}_{\Lambda 1}$ is the effective cross section for the process corresponding to $\Lambda_1 = 1\,\text{TeV}$, given in units of fb TeV^4. The cross-section ratios are quoted in Table 1. The a_i/a_1 ratios can be obtained from the ratio f_{ai}/f_{a1}, the cross-section ratios, and the phase ϕ_{ai} as

$$\frac{a_i}{a_1} = \sqrt{\frac{f_{ai}}{f_{a1}}\frac{\sigma_1}{\sigma_i}}\,e^{i\phi_{ai}}. \tag{5}$$

The effective fractions f_{ai} are bounded between 0 and 1 and do not depend on the coupling convention. In most cases, uncertainties on these measurements scale with integrated luminosity as $1/\sqrt{\mathcal{L}}$ until effects of interference become important. Furthermore, the values of f_{ai} have a simple interpretation as the fractional size of the BSM contribution for the $H \to 2e2\mu$ decay. For example, $f_{ai} = 0$ indicates a pure SM-like H boson, $f_{ai} = 1$ gives a pure BSM particle, and $f_{ai} = 0.5$ means that the two couplings contribute equally to the $H \to 2e2\mu$ process.

As mentioned above in application to Eq. (3), the measurement of f_{ai} is performed under the $r_{ai} = 1$ assumption. Let us denote this to be an effective f_{ai}^{eff}. Without such an assumption, there is a certain dependence of f_{ai} on r_{ai} and f_{ai}^{eff}, such that $f_{ai} = f_{ai}^{\text{eff}}$ for $r_{ai} = 1$. This dependence is different for different processes, such as VBF production or $H \to 4\ell$ decay, where the latter

Table 1: List of the anomalous HVV couplings considered in the measurements assuming a spin-zero H boson. The definition of the effective fractions f_{ai} is discussed in the text and the translation constants are the cross-section ratios corresponding to the processes $H \to 2e2\mu$ with the H boson mass $m_H = 125\,\text{GeV}$ and calculated using JHUGEN [47, 50, 54].

Anomalous Coupling	Coupling Phase	Effective Fraction	Translation Constant
a_3	ϕ_{a3}	f_{a3}	$\sigma_1/\sigma_3 = 6.53$
a_2	ϕ_{a2}	f_{a2}	$\sigma_1/\sigma_2 = 2.77$
Λ_1	$\phi_{\Lambda 1}$	$f_{\Lambda 1}$	$\sigma_1/\tilde{\sigma}_{\Lambda 1} = 1.47 \times 10^4\,\text{TeV}^{-4}$
$\Lambda_1^{Z\gamma}$	$\phi_{\Lambda 1}^{Z\gamma}$	$f_{\Lambda 1}^{Z\gamma}$	$\sigma_1/\tilde{\sigma}_{\Lambda 1}^{Z\gamma} = 5.80 \times 10^3\,\text{TeV}^{-4}$

case is in fact independent of r_{ai} because the HWW coupling does not affect this decay process. In the former case, let us consider the relative contributions of WW and ZZ fusion on-shell. For example, the ratio of VBF cross sections driven by WW and ZZ fusion is $\sigma_1^{WW}/\sigma_1^{ZZ} = 2.59$ for the SM tree-level couplings under custodial symmetry $a_1^{WW} = a_1^{ZZ}$ at 13 TeV pp collision energy. The same ratio for the CP-odd couplings is $\sigma_3^{WW}/\sigma_3^{ZZ} = 3.15$, where σ_3^{VV} are calculated for $a_3^{WW} = a_3^{ZZ}$. The dependence of f_{ai} on r_{ai} and f_{ai}^{eff}, as measured in the VBF process, becomes

$$f_{ai} = \left[1 + (1/f_{ai}^{\text{eff}} - 1)(\sigma_i^{ZZ} + \sigma_i^{WW})/(\sigma_i^{ZZ} + r_{ai}^2\sigma_i^{WW})\right]^{-1}, \tag{6}$$

where custodial symmetry $a_1^{WW} = a_1^{ZZ}$ is assumed and the effects of interference between WW and ZZ fusion are negligible and are therefore ignored.

All of the above discussion, including Eq. (2), describes the production of a resonance via gluon fusion, VBF with associated jets, or associated production with an EW vector boson, VH. These mechanisms, along with the $t\bar{t}H$ and $b\bar{b}H$ production, are considered in the analysis of the spin-zero hypothesis of the H boson, where the gluon fusion production is expected to dominate. It is possible to study HVV interactions using the kinematics of particles produced in association with the H boson, such as VBF jets or vector boson daughters in VH production, as we show below. More details can be found in, e.g., Ref. [54] and the experimental application in Refs. [26, 27]. While the q_i^2 range in the HVV process does not exceed approximately 100 GeV because of the kinematic bound, no such bound exists in the associated production, so consideration of more restricted q_i^2 ranges might be required [54]. However, we only consider that the q_i^2 range is not restricted in the allowed phase space.

3 The CMS detector, simulation, and reconstruction

The $H \to 4\ell$ decay candidates are reconstructed in the CMS detector [60]. The CMS detector is comprised of a silicon pixel and strip tracker, a lead tungstate crystal electromagnetic calorimeter (ECAL), and a brass/scintillator hadron calorimeter, each composed of a barrel and two endcap sections, all within a superconducting solenoid of 6 m internal diameter, providing a magnetic field of 3.8 T. Extensive forward calorimetry complements the coverage provided by the barrel and endcap detectors. Outside the solenoid are the gas-ionization detectors for muon measurements, which are embedded in the steel flux-return yoke. A detailed description of the CMS detector, together with a definition of the coordinate system used and the relevant kinematic variables, can be found in Ref. [60].

The JHUGEN 7.0.2 [47, 50, 54, 59] Monte Carlo (MC) program is used to simulate anomalous couplings in the H boson production and $H \to ZZ$ / $Z\gamma^*$ / $\gamma^*\gamma^* \to 4\ell$ decay. The gluon fusion

production is simulated with the POWHEG 2 [61–65] event generator at next-to-leading order (NLO) in QCD, and simulation with the MINLO [66] program at NLO in QCD is used for evaluation of systematic uncertainties related to modeling of two associated jets. The kinematics of events produced in gluon fusion with two associated jets are also modified by anomalous Hgg couplings. These effects are studied using JHUGEN, and it is found that the kinematic distributions relevant for this analysis are not affected significantly.

The production of the H boson through VBF, in association with a W or Z boson, or with a $\mathrm{t\bar{t}}$ pair, is simulated using both JHUGEN at LO in QCD and POWHEG at NLO in QCD. Production in association with a $\mathrm{b\bar{b}}$ pair is simulated only at LO in QCD via JHUGEN. In the VBF, VH, and $\mathrm{t\bar{t}H}$ production modes, the JHUGEN and POWHEG simulations are explicitly compared after parton showering in the SM case, and no significant differences are found in kinematic observables. Therefore, the JHUGEN simulation is adopted to describe kinematics in the VBF, VH, and $\mathrm{t\bar{t}H}$ production modes with anomalous couplings in the on-shell region, with expected yields taken from the POWHEG simulation. The POWHEG program is used to simulate wide resonances at masses ranging from 115 GeV to 3 TeV, produced in gluon fusion, VBF, or VH. The events from the POWHEG simulation are later reweighted using the package for the matrix element likelihood approach (MELA) [9, 47, 50, 54, 59] to model off-shell H boson production distributions, as discussed below.

The $\mathrm{gg} \to \mathrm{ZZ}/\mathrm{Z}\gamma^* \to 4\ell$ background process is simulated with MCFM 7.0.1 [18, 67–69]. The vector boson scattering and triple-gauge-boson (VVV) backgrounds are obtained by reweighting the POWHEG simulation with the matrix elements provided by the MELA package using the MCFM and JHUGEN matrix elements, and the reweighted simulation is checked against the predictions of the PHANTOM 1.3 [70] simulation. Both the MCFM and PHANTOM generators allow one to model the H boson signal, background, and their interference in the off-shell production. However, they do not allow modeling of the anomalous interactions considered in this analysis. Therefore, a combined program has been developed for both gluon fusion and VBF with triple-gauge-boson production based on the modeling of signal and background scattering amplitudes from MCFM and anomalous contributions in the signal scattering amplitude from JHUGEN. This program is included within the JHUGEN and MELA packages, as detailed in Ref. [22]. A large number of MC events with anomalous couplings in the signal and their interference with background have been generated with these packages. The simulated events also include alternative weights to model various anomalous couplings in the signal.

In the gluon fusion process, the factorization and renormalization scales are chosen to be running as $m_{4\ell}/2$. In order to include higher-order QCD corrections, LO, NLO, and next-to-NLO (NNLO) signal cross section calculations are performed using the MCFM and HNNLO 2 programs [71–73] for a wide range of masses using a narrow width approximation. The ratios between the NNLO and LO values (NNLO K factors) are used to reweight [22] the $m_{4\ell}$ distributions from the MCFM and JHUGEN simulation at LO in QCD, and a uniform factor of 1.10 across all of the $m_{4\ell}$ range is applied to normalize the cross section of the H boson production via gluon fusion to the predictions for $m_{4\ell} \approx 125\,\mathrm{GeV}$ at next-to-NNLO (N^3LO) in QCD [22]. The simulated $m_{4\ell}$ shapes or yields obtained from the POWHEG simulation of the gluon fusion process are corrected based on the above reweighted distributions. While the NNLO K factor calculation is directly applicable to the signal contribution, it is approximate for the background and its interference with the signal. The NLO calculation with some approximations [74–77] is available for the background and interference. Comparison with this calculation shows that while there is some increase of the NLO K factor for the interference close to the ZZ threshold, the NLO K factors for the background and interference are consistent with the signal within approximately 10% in the mass range $m_{4\ell} > 220\,\mathrm{GeV}$ relevant for this analysis. We therefore

multiply the background and interference contributions by the same NNLO K factor and uniform N^3LO correction, both calculated for signal and including associated uncertainties, and introduce an additional unit factor with a 10% uncertainty for the background and the square root of this factor for the interference.

The MELA package contains a library of matrix elements from JHUGEN and MCFM for the signal, and MCFM for the background, and is used to apply weights to events in any MC sample to model any other set of anomalous or SM couplings in either on-shell or off-shell production. This matrix element library also allows reweighting of the signal POWHEG simulation of the wide resonances at NLO in QCD in either gluon fusion, VBF, or triple-gauge-boson production to model the signal, background, or their interference.

The main background in this analysis, $q\bar{q} \to ZZ/Z\gamma^* \to 4\ell$, is estimated from simulation with POWHEG. A fully differential cross section has been computed at NNLO in QCD [78], but it is not yet available in a partonic level event generator. Therefore the NNLO/NLO QCD correction is applied as a function of $m_{4\ell}$. Additional NLO EW corrections are also applied to this background process in the region $m_{4\ell} > 2m_Z$ [79, 80]. The parton distribution functions (PDFs) used in this paper belong to the NNPDF 3.0 PDF sets [81]. All MC samples are interfaced to PYTHIA 8 [82] for parton showering, using version 8.212 for the simulation of the 2016 data period and 8.230 for the simulation of the 2017 data period. Simulated events include the contribution from additional pp interactions within the same or adjacent bunch crossings (pileup), and are weighted to reproduce the observed pileup distribution. The MC samples are further processed through a dedicated simulation of the CMS detector based on GEANT4 [83].

The selection of 4ℓ events and associated particles closely follows the methods used in the analyses of the Run 1 [24] and Run 2 [21] data sets. The main triggers for the Run 2 analysis select either a pair of electrons or muons, or an electron and a muon. The minimal transverse momentum of the leading electron (muon) is 23 (17) GeV, while that of the subleading lepton is 12 (8) GeV. To maximize the signal acceptance, triggers requiring three leptons with lower p_T thresholds and no isolation requirement are also used, as are isolated single-electron and single-muon triggers with thresholds of 27 and 22 GeV in 2016, or 35 and 27 GeV in 2017, respectively. The overall trigger efficiency for simulated signal events that pass the full selection chain of this analysis is larger than 99%. The trigger efficiency is measured in data using a sample of 4ℓ events collected by the single-lepton triggers and is found to be consistent with the expectation from simulation.

Event reconstruction is based on the particle-flow (PF) algorithm [84], which exploits information from all the CMS subdetectors to identify and reconstruct individual particles in the event. The PF candidates are classified as charged hadrons, neutral hadrons, photons, electrons, or muons, and they are then used to build higher-level objects such as jets and lepton isolation quantities. Electrons (muons) are reconstructed within the geometrical acceptance defined by a requirement on the pseudorapidity $|\eta| < 2.5\,(2.4)$ for transverse momentum $p_T > 7\,(5)$ GeV with an algorithm that combines information from the ECAL (muon system) and the tracker. A dedicated algorithm is used to collect the final-state radiation (FSR) of leptons [21].

The reconstructed vertex with the largest value of summed physics-object p_T^2 is taken to be the primary pp interaction vertex. The physics objects are the jets and the associated missing transverse momentum, taken as the negative vector sum of the p_T of those jets. The jets are clustered using the anti-k_T jet finding algorithm [85, 86] with a distance parameter of 0.4 and the associated tracks assigned to the vertex as inputs. Jets must satisfy $p_T > 30$ GeV and $|\eta| < 4.7$ and must be separated from all selected lepton candidates and any selected FSR photons with a requirement on the distance parameter $\Delta R(\ell/\gamma, \text{jet}) > 0.4$, where $(\Delta R)^2 = (\Delta\phi)^2 + (\Delta\eta)^2$.

For event categorization, jets are tagged as b-jets using the Combined Secondary Vertex algorithm [87, 88], which combines information about impact parameter significance, the secondary vertex, and jet kinematics.

We require each lepton track to have the ratio of the impact parameter in three dimensions, computed with respect to the chosen primary vertex position, and its uncertainty to be less than 4. To discriminate prompt leptons from Z boson decays from those arising from hadron decays within jets, an isolation requirement for leptons is imposed [21]. We consider three mutually exclusive channels: $\mathrm{H} \to 4\mathrm{e}$, 4μ, and $2\mathrm{e}2\mu$. At least two leptons are required to have $p_{\mathrm{T}} > 10\,\mathrm{GeV}$, and at least one is required to have $p_{\mathrm{T}} > 20\,\mathrm{GeV}$. All four pairs of oppositely charged leptons that can be built with the four leptons are required to satisfy $m_{\ell^+\ell'^-} > 4\,\mathrm{GeV}$ regardless of lepton flavor. The Z candidates are required to satisfy the condition $12 < m_{\ell^+\ell^-} < 120\,\mathrm{GeV}$, where the invariant mass of at least one of the Z candidates must be larger than 40 GeV. The four-lepton invariant mass $m_{4\ell}$ must be between 105 and 140 GeV in the on-shell region and above 220 GeV in the off-shell region.

4 Analysis techniques and categorization of events

The full kinematic information from each event using either the H boson decay or associated particles in its production is extracted using discriminants from matrix element calculations. These discriminants use a complete set of mass and angular input observables $\boldsymbol{\Omega}$ [47, 54, 59] to describe kinematics at LO in QCD. The p_{T} of either the combined H boson and two-jet system for the production discriminant (e.g., $\mathcal{D}^{\mathrm{VBF/VH}}$), or the H boson itself for the decay discriminants (e.g., $\mathcal{D}^{\mathrm{dec}}$), or for their combination (e.g., $\mathcal{D}^{\mathrm{VBF/VH+dec}}$) is not included in the input observables. This information is not used in the analysis of the H boson width and anomalous couplings, as the p_{T} of the overall system is sensitive to QCD, parton shower, and underlying event uncertainties.

The kinematic discriminants used in this study are computed using the same MELA package that is utilized in simulation. The signal includes both the four-lepton decay kinematics in the processes $\mathrm{H} \to \mathrm{ZZ}$ / $\mathrm{Z}\gamma^*$ / $\gamma^*\gamma^* \to 4\ell$, and kinematics of associated particles in production H+jet, H+2jets, VBF, WH, ZH, $\mathrm{t\bar{t}H}$, tqH, or $\mathrm{b\bar{b}H}$. The background includes gg or $\mathrm{q\bar{q}} \to \mathrm{ZZ}$ / $\mathrm{Z}\gamma^*$ / $\gamma^*\gamma^*$ / $\mathrm{Z} \to 4\ell$ processes, and VBF or associated production with a V boson of the ZZ system. Analytical algorithms are available for the cross-checks of the four-lepton kinematics in H decay and VH associated production within the MELA framework and were adopted in the previous CMS analyses [9, 10, 23].

Kinematic distributions of particles produced in the H boson decay or in association with H boson production are sensitive to the quantum numbers and anomalous couplings of the H boson. In the $1 \to 4$ process of the $\mathrm{H} \to 4\mathrm{f}$ decay, six observables fully characterize kinematics of the decay products $\boldsymbol{\Omega}^{\mathrm{decay}} = \{\theta_1, \theta_2, \Phi, m_1, m_2, m_{4\mathrm{f}}\}$, while two other angles relate orientation of the decay frame with respect to the production axis, $\boldsymbol{\Omega}^{\mathrm{prod}} = \{\theta^*, \Phi_1\}$, as described in Ref. [47]. Moreover, two sets of observables, $\boldsymbol{\Omega}^{\mathrm{assoc,\,VBF}} = \{\theta_1^{\mathrm{VBF}}, \theta_2^{\mathrm{VBF}}, \Phi^{\mathrm{VBF}}, q_1^{2,\mathrm{VBF}}, q_2^{2,\mathrm{VBF}}\}$ for the VBF process and $\boldsymbol{\Omega}^{\mathrm{assoc,\,VH}} = \{\theta_1^{\mathrm{VH}}, \theta_2^{\mathrm{VH}}, \Phi^{\mathrm{VH}}, q_1^{2,\mathrm{VH}}, q_2^{2,\mathrm{VH}}\}$ for the VH process, can also be defined in a similar way to $\boldsymbol{\Omega}^{\mathrm{decay}}$ for H boson associated production [54]. As a result, 13 kinematic observables, illustrated in Fig. 1, are defined for the $2 \to 6$ associated production process with subsequent H boson decay to a four-fermion final state.

With up to 13 observables, $\boldsymbol{\Omega}$, sensitive to the H boson anomalous couplings in Eq. (2), it is a challenging task to perform an optimal analysis in a multidimensional space of observables. The MELA approach introduced earlier is designed to reduce the number of observables to the

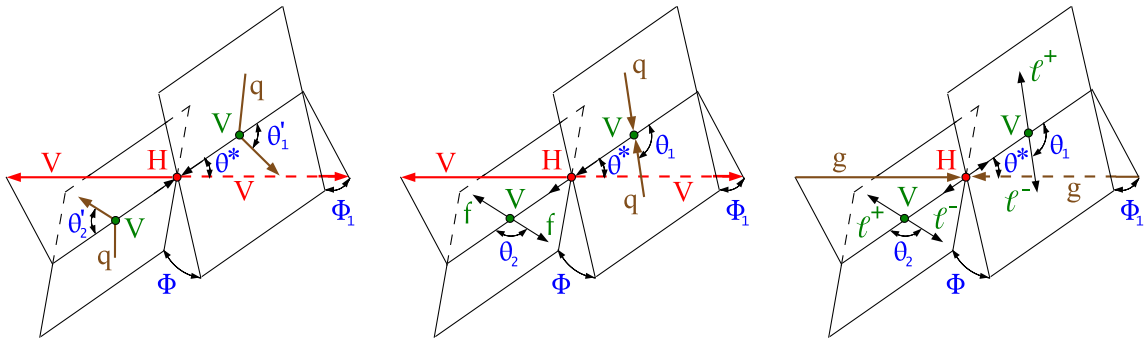

Figure 1: Three topologies of the H boson production and decay: vector boson fusion $qq \to VV(qq) \to H(qq) \to VV(qq)$ (left); associated production $qq \to V \to VH \to (f\bar{f})\ H \to (f\bar{f})\ VV$ (middle); and gluon fusion $gg \to H \to VV \to 4\ell$ (right) representing the topology without associated particles. The incoming particles are shown in brown, the intermediate vector bosons and their fermion daughters are shown in green, the H boson and its vector boson daughters are shown in red, and angles are shown in blue. In the first two cases the production and decay $H \to VV$ are followed by the same four-lepton decay shown in the third case. The angles are defined in either the H or V boson rest frames [47, 54].

minimum while retaining all essential information. Two types of discriminants were defined for either the production or decay process, and we also combine them into a joint discriminant for the full $2 \to 6$ process where relevant.

These types of discriminants are

$$\mathcal{D}_{\text{alt}}\left(\mathbf{\Omega}\right) = \frac{\mathcal{P}_{\text{sig}}\left(\mathbf{\Omega}\right)}{\mathcal{P}_{\text{sig}}\left(\mathbf{\Omega}\right) + \mathcal{P}_{\text{alt}}\left(\mathbf{\Omega}\right)} \tag{7}$$

and

$$\mathcal{D}_{\text{int}}\left(\mathbf{\Omega}\right) = \frac{\mathcal{P}_{\text{int}}\left(\mathbf{\Omega}\right)}{2\sqrt{\mathcal{P}_{\text{sig}}\left(\mathbf{\Omega}\right)\ \mathcal{P}_{\text{alt}}\left(\mathbf{\Omega}\right)}}, \tag{8}$$

where the probability of a certain process $\mathcal{P}$ is calculated using the full kinematics characterized by $\mathbf{\Omega}$ for the processes denoted as "sig" for a signal model and "alt" for an alternative model, which could be an alternative H boson production mechanism (used to categorize events), background (to isolate signal), or an alternative H boson coupling model (to measure coupling parameters). The "int" label represents the interference between the two model contributions. The probabilities $\mathcal{P}$ are calculated from the matrix elements provided by the MELA package and are normalized to give the same integrated cross sections in the relevant phase space of each process. Such normalization leads to a balanced distribution of events in the range between 0 and 1 of the $\mathcal{D}_{\text{alt}}$ discriminants, and between -1 and 1 of $\mathcal{D}_{\text{int}}$. One can apply the Neyman-Pearson lemma to prove that the two discriminants in Eqs. (7) and (8) become the minimal and complete set of optimal observables for the purpose of separating the two processes "sig" and "alt" while including their interference as well [54, 59].

The selected events are split into three categories: VBF-tagged, VH-tagged, and untagged. A set of discriminants $\mathcal{D}_{\text{2jet}}$ is constructed, following Eq. (7), where $\mathcal{P}_{\text{sig}}$ corresponds to the signal probability for the VBF (WH or ZH) production hypothesis in the VBF-tagged (VH-tagged) category, and $\mathcal{P}_{\text{alt}}$ corresponds to that of H boson production in association with two jets via gluon fusion. Thereby, the $\mathcal{D}_{\text{2jet}}$ discriminants separate the target production mode of each category from gluon fusion production, in all cases using only the kinematics of the H boson and two associated jets. When more than two jets pass the selection criteria, the two jets with

the highest p_T are chosen for the matrix element calculations. The three on-shell and off-shell categories and their sequential selection criteria are summarized in Tables 2 and 3, and are as follows:

- VBF-*tagged* requires exactly four leptons, either two or three jets of which at most one is b-quark flavor-tagged, or more if none are b-tagged jets, and $\mathcal{D}_{2jet}^{VBF} > 0.5$ using either the SM or BSM signal hypothesis for the VBF production.
- VH-*tagged* requires exactly four leptons, either two or three jets, or more if none are b-tagged jets, and $\mathcal{D}_{2jet}^{VH} = \max\left(\mathcal{D}_{2jet}^{WH}, \mathcal{D}_{2jet}^{ZH}\right) > 0.5$ using either the SM or BSM signal hypothesis for the VH production.
- *Untagged* consists of the remaining events.

The requirements on the number of b-tagged jets are applied to reduce crossfeed from $t\bar{t}H$ production. Even though VH cross sections are significantly lower with respect to VBF for $m_{4\ell} > 220\,\text{GeV}$, the VH cross section becomes comparable to the VBF cross section in the presence of anomalous couplings. Therefore, the off-shell analysis also benefits from featuring the VH-tagged category with hadronic decays of the associated V. In either the on-shell or off-shell regions, events are not tagged for the smaller VH contribution with leptonic V decays explicitly, but this contribution is taken into account in the simulation and parameterization of the VH process in the three different categories. The expected and observed numbers of events are listed in Table 4 for the on-shell region and Table 5 for the off-shell region.

Table 2: Summary of the three production categories in the on-shell $m_{4\ell}$ region. The selection requirements on the $\mathcal{D}_{2jet}$ discriminants are quoted for each category, and further requirements can be found in the text. Two or three observables (abbreviated as obs.) are listed for each analysis and for each category. All discriminants are calculated with the JHUGEN signal matrix elements and MCFM background matrix elements. The discriminants $\mathcal{D}_{bkg}$ in the tagged categories also include probabilities using associated jets and decay in addition to the $m_{4\ell}$ probability. The VH interference discriminants in the hadronic VH-tagged categories are defined as the simple average of the ones corresponding to the WH and ZH processes.

Category	VBF-tagged	VH-tagged	Untagged
Selection	$\mathcal{D}_{2jet}^{VBF}$ or $\mathcal{D}_{2jet}^{VBF,BSM} > 0.5$	$\mathcal{D}_{2jet}^{WH}$ or $\mathcal{D}_{2jet}^{WH,BSM}$, or $\mathcal{D}_{2jet}^{ZH}$ or $\mathcal{D}_{2jet}^{ZH,BSM} > 0.5$	Rest of events
SM obs.	$m_{4\ell}$, $\mathcal{D}_{bkg}^{VBF+dec}$	$m_{4\ell}$, $\mathcal{D}_{bkg}^{VH+dec}$	$m_{4\ell}$, $\mathcal{D}_{bkg}^{kin}$
a_3 obs.	$\mathcal{D}_{bkg}$, $\mathcal{D}_{0-}^{VBF+dec}$, $\mathcal{D}_{CP}^{VBF}$	$\mathcal{D}_{bkg}$, $\mathcal{D}_{0-}^{VH+dec}$, $\mathcal{D}_{CP}^{VH}$	$\mathcal{D}_{bkg}$, $\mathcal{D}_{0-}^{dec}$, $\mathcal{D}_{CP}^{dec}$
a_2 obs.	$\mathcal{D}_{bkg}$, $\mathcal{D}_{0h+}^{VBF+dec}$, $\mathcal{D}_{int}^{VBF}$	$\mathcal{D}_{bkg}$, $\mathcal{D}_{0h+}^{VH+dec}$, $\mathcal{D}_{int}^{VH}$	$\mathcal{D}_{bkg}$, $\mathcal{D}_{0h+}^{dec}$, $\mathcal{D}_{int}^{dec}$
Λ_1 obs.	$\mathcal{D}_{bkg}$, $\mathcal{D}_{\Lambda 1}^{VBF+dec}$, $\mathcal{D}_{0h+}^{VBF+dec}$	$\mathcal{D}_{bkg}$, $\mathcal{D}_{\Lambda 1}^{VH+dec}$, $\mathcal{D}_{0h+}^{VH+dec}$	$\mathcal{D}_{bkg}$, $\mathcal{D}_{\Lambda 1}^{dec}$, $\mathcal{D}_{0h+}^{dec}$
$\Lambda_1^{Z\gamma}$ obs.	$\mathcal{D}_{bkg}$, $\mathcal{D}_{\Lambda 1}^{Z\gamma,VBF+dec}$, $\mathcal{D}_{0h+}^{VBF+dec}$	$\mathcal{D}_{bkg}$, $\mathcal{D}_{\Lambda 1}^{Z\gamma,VH+dec}$, $\mathcal{D}_{0h+}^{VH+dec}$	$\mathcal{D}_{bkg}$, $\mathcal{D}_{\Lambda 1}^{Z\gamma,dec}$, $\mathcal{D}_{0h+}^{dec}$

In each category of events, typically three observables $\vec{x}$ are defined following Eqs. (7) and (8), as summarized in Tables 2 and 3. In the on-shell region, except for the SM-like analysis, these are $\vec{x} = \{\mathcal{D}_{bkg}, \mathcal{D}_{ai}, \mathcal{D}_{int}\}$. The first observable, $\mathcal{D}_{bkg}$, is calculated differently in the three tagged categories. In the untagged category, $\mathcal{P}_{bkg}$ is calculated for the dominant $q\bar{q} \to 4\ell$ background process. The signal and background probabilities include both the matrix element probability based on the four-lepton kinematics and the $m_{4\ell}$ probability parameterization extracted from

Table 3: Summary of the three production categories in the off-shell $m_{4\ell}$ region, listed in a similar manner, as in Table 2. All discriminants are calculated with the JHUGEN or MCFM/JHUGEN signal, and MCFM background matrix elements. The VH interference discriminant in the SM-like analysis hadronic VH-tagged category is defined as the simple average of the ones corresponding to the WH and ZH processes.

Category	VBF-tagged	VH-tagged	Untagged
Selection	$\mathcal{D}_{2\text{jet}}^{\text{VBF}}$ or $\mathcal{D}_{2\text{jet}}^{\text{VBF,BSM}} > 0.5$	$\mathcal{D}_{2\text{jet}}^{\text{WH}}$ or $\mathcal{D}_{2\text{jet}}^{\text{WH,BSM}}$, or $\mathcal{D}_{2\text{jet}}^{\text{ZH}}$ or $\mathcal{D}_{2\text{jet}}^{\text{ZH,BSM}} > 0.5$	Rest of events
SM obs.	$m_{4\ell}$, $\mathcal{D}_{\text{bkg}}^{\text{VBF+dec}}$, $\mathcal{D}_{\text{bsi}}^{\text{VBF+dec}}$	$m_{4\ell}$, $\mathcal{D}_{\text{bkg}}^{\text{VH+dec}}$, $\mathcal{D}_{\text{bsi}}^{\text{VH+dec}}$	$m_{4\ell}$, $\mathcal{D}_{\text{bkg}}^{\text{kin}}$, $\mathcal{D}_{\text{bsi}}^{\text{gg,dec}}$
a_3 obs.	$m_{4\ell}$, $\mathcal{D}_{\text{bkg}}^{\text{VBF+dec}}$, $\mathcal{D}_{0-}^{\text{VBF+dec}}$	$m_{4\ell}$, $\mathcal{D}_{\text{bkg}}^{\text{VH+dec}}$, $\mathcal{D}_{0-}^{\text{VH+dec}}$	$m_{4\ell}$, $\mathcal{D}_{\text{bkg}}^{\text{kin}}$, $\mathcal{D}_{0-}^{\text{dec}}$
a_2 obs.	$m_{4\ell}$, $\mathcal{D}_{\text{bkg}}^{\text{VBF+dec}}$, $\mathcal{D}_{0h+}^{\text{VBF+dec}}$	$m_{4\ell}$, $\mathcal{D}_{\text{bkg}}^{\text{VH+dec}}$, $\mathcal{D}_{0h+}^{\text{VH+dec}}$	$m_{4\ell}$, $\mathcal{D}_{\text{bkg}}^{\text{kin}}$, $\mathcal{D}_{0h+}^{\text{dec}}$
Λ_1 obs.	$m_{4\ell}$, $\mathcal{D}_{\text{bkg}}^{\text{VBF+dec}}$, $\mathcal{D}_{\Lambda 1}^{\text{VBF+dec}}$	$m_{4\ell}$, $\mathcal{D}_{\text{bkg}}^{\text{VH+dec}}$, $\mathcal{D}_{\Lambda 1}^{\text{VH+dec}}$	$m_{4\ell}$, $\mathcal{D}_{\text{bkg}}^{\text{kin}}$, $\mathcal{D}_{\Lambda 1}^{\text{dec}}$

Table 4: The numbers of events expected in the SM (or $f_{a3} = 1$ in parentheses) for the different signal and background contributions and the total numbers of observed events are listed across the three a_3 analysis categories in the on-shell region for the combined 2016 and 2017 data set.

	VBF-tagged	VH-tagged	Untagged
VBF signal	4.7 (3.4)	0.3 (0.2)	5.7 (0.8)
WH signal	0.3 (0.6)	0.7 (1.9)	2.1 (5.3)
ZH signal	0.2 (0.4)	0.5 (1.0)	1.5 (2.5)
VV background	0.2	0.1	0.5
gg signal	5.5 (5.8)	3.2 (3.3)	98.9 (98.4)
gg background	0.8	0.3	12.7
$\mathrm{t\bar{t}H}$ signal	0.2 (0.2)	0.1 (0.1)	1.1 (1.2)
$\mathrm{b\bar{b}H}$ signal	0.1 (0.1)	0.1 (0.1)	1.1 (1.1)
$\mathrm{q\bar{q}} \to 4\ell$ background	1.6	1.5	120.3
$\mathrm{Z} + \mathrm{X}$ background	5.2	3.0	46.3
Total expected	18.8 (18.2)	9.7 (11.4)	290.3 (289.1)
Total observed	19	9	332

Table 5: The numbers of events expected in the SM-like analysis (or $f_{a3} = 0$ in the a_3 analysis categorization, divided with a vertical bar) for the different signal and background contributions and the total observed numbers of events are listed across the three SM | a_3 analysis categories in the off-shell region for the combined 2016 and 2017 data set. The signal, background, and interference contributions are shown separately for the gluon fusion (gg) and EW processes (VV) under the $\Gamma_H = \Gamma_H^{SM}$ assumption.

	VBF-tagged	VH-tagged	Untagged
VV signal	1.0 | 1.2	0.3 | 0.3	3.3 | 3.1
VV background	7.3 | 9.9	2.5 | 2.8	16.2 | 13.3
VV interference	−1.8 | −2.1	0.06 | 0.03	−2.4 | −2.2
gg signal	1.0 | 1.6	0.8 | 1.0	20.3 | 19.5
gg background	10.4 | 16.4	8.7 | 10.4	245.9 | 238.1
gg interference	−1.6 | −2.6	−1.4 | −1.6	−34.4 | −33.0
$q\bar{q} \to 4\ell$ background	15.8 | 33.5	27.8 | 31.2	992.0 | 970.8
Z + X background	2.4 | 6.4	2.8 | 3.3	45.4 | 40.8
Total expected	34.4 | 64.8	41.6 | 47.5	1286.3 | 1251.0
Total observed	36 | 92	46 | 51	1325 | 1264

simulation of detector effects. The signal $m_{4\ell}$ parameterization assumes $m_H = 125\,\text{GeV}$. In the VBF-tagged and VH-tagged categories, $\mathcal{P}_{bkg}$ and $\mathcal{P}_{sig}$ include four-lepton kinematics and the $m_{4\ell}$ probability parameterization, but they also include kinematics of the two associated jets. The $\mathcal{P}_{bkg}$ probability density represents the EW and QCD background processes $4\ell + 2\,\text{jets}$, while $\mathcal{P}_{sig}$ represents EW processes VBF and VH. It was found that jet kinematics in the $\mathcal{D}_{bkg}$ calculation improves separation of the targeted signal production both against background and against the H boson gluon fusion production. However, in the off-shell region and in the SM-like on-shell analysis, the four-lepton invariant mass $m_{4\ell}$ is one of the most important observables, because the mass parameterization becomes an important feature of the analysis. Therefore, the $m_{4\ell}$ parameterization is not used in the $\mathcal{D}_{bkg}$ calculation in these cases, and this is reflected with the superscript denoting which information is used, either with decay only information in $\mathcal{D}_{bkg}^{kin}$ or with both decay and production in $\mathcal{D}_{bkg}^{VBF+dec}$ and $\mathcal{D}_{bkg}^{VH+dec}$.

The other observable, $\mathcal{D}_{ai}$, separates the SM hypothesis $f_{ai} = 0$ as $\mathcal{P}_{sig}$ from the alternative hypothesis $f_{ai} = 1$ as $\mathcal{P}_{alt}$, following Eq. (7). In the untagged category, the probabilities are calculated using only the decay information, and the $\mathcal{D}_{ai}$ observable is called $\mathcal{D}_{0-}$ in the a_3, $\mathcal{D}_{0h+}$ in the a_2, $\mathcal{D}_{\Lambda 1}$ in the Λ_1, and $\mathcal{D}_{\Lambda 1}^{Z\gamma}$ in the $\Lambda_1^{Z\gamma}$ analyses [25]. In the VBF-tagged and VH-tagged categories, both the production and decay probabilities are used, with the matrix elements calculated as the product of the decay component and the component from either VBF production or $(WH + ZH)$ associated production, respectively [27]. The resultant set of $\mathcal{D}_{ai}$ discriminants are called in a similar manner to their counterparts in the untagged category but indicating the production assumption in their upper index.

The last observable, $\mathcal{D}_{int}$ defined in Eq. (8), separates the interference of the two amplitudes corresponding to the SM-like H boson coupling and the alternative H boson coupling model, or the SM-like H boson coupling and background as an alternative model in the case of $\mathcal{D}_{bsi}$ for the signal-background interference in the off-shell region. In the case of the a_3 analysis, this observable is called $\mathcal{D}_{CP}$ because if CP is violated it would exhibit a distinctive forward-backward asymmetry. In the untagged category, decay information is used in the calculation of $\mathcal{D}_{int}$. In the VBF-tagged and VH-tagged categories, production information with the two

associated jets is used. The $\mathcal{D}_{\text{bsi}}$ discriminant extends the idea of the $\mathcal{D}_{\text{gg}}$ discriminant introduced in Ref. [11] for the H boson width measurement, but allows independent treatment of the interference component. It is used only in the SM-like analysis.

5 Kinematic distributions and the fit implementation

We perform an unbinned extended maximum likelihood fit [89] to the events split into several categories (enumerated with an index k below) according to the three lepton flavor combinations (4e, 4μ, and 2e2μ), three production categories (VBF-tagged, VH-tagged, and untagged), five data periods (2011, 2012, 2015, 2016, and 2017), and two mass ranges (on-shell and off-shell). Therefore, there could be up to 90 categories of events. However, not all categories are used in each independent measurement because of the simpler categorization approach applied to the earlier data. Here we focus on discussion of the 2016 and 2017 data analyses, while treatment of the earlier data can be found in Refs. [13, 25, 27].

An independent fit is performed for each of the four anomalous HVV coupling parameters $f_{ai}\cos(\phi_{ai})$ using the on-shell region only. These fits avoid any assumptions on how the behavior of each process considered in the analysis changes from the on-shell region to the off-shell region. The $\Lambda_1^{\text{Z}\gamma}$ coupling is considered only in the on-shell analysis because there is no longer an interplay between the on-shell and off-shell regions when the intermediate boson is a virtual photon. Four independent joint fits to the on-shell and off-shell regions are performed in order to determine the width of the H boson under the SM-like or three remaining anomalous coupling assumptions. These fits are also used to constrain three anomalous coupling parameters $f_{ai}\cos(\phi_{ai})$. When a certain anomalous coupling is tested, all other anomalous couplings are assumed to be zero, and only real couplings in Eq. (2) are tested, that is $\cos(\phi_{ai}) = \pm 1$.

The on-shell analysis with the study of the a_3, a_2, Λ_1, and $\Lambda_1^{\text{Z}\gamma}$ couplings has been presented in Ref. [27] using a partial data set. This part of the analysis remains essentially unchanged, except for a small change in the definition of the interference discriminant in Eq. (8) and the inclusion of information from the kinematics of the two associated jets in the $\mathcal{D}_{\text{bkg}}$ calculation discussed in Section 4. The SM-like on-shell analysis is similar to the one presented in Ref. [21] in methodology, but it uses the observables $\vec{x}$ and categorization k described in Table 2 and Section 4. The on-shell probability density is normalized to the total event yield in each process j and category k according to

$$\mathcal{P}_{jk}(\vec{x};\vec{\xi}_{jk},\vec{\zeta}) = \mu_j \mathcal{P}_{jk}^{\text{sig}}\left(\vec{x};\vec{\xi}_{jk},f_{ai},\phi_{ai}\right) + \mathcal{P}_{jk}^{\text{bkg}}\left(\vec{x};\vec{\xi}_{jk}\right), \tag{9}$$

where $\vec{\zeta} = (\mu_{\text{F}}, \mu_{\text{V}}, \Gamma_{\text{H}}, f_{ai}\cos(\phi_{ai}))$ are the unconstrained parameters of interest, $\vec{\xi}_{jk}$ are the constrained nuisance parameters for a particular parameterization, and $\vec{x}$ are the observables listed in Table 2, specific to each a_i. The on-shell signal strength μ_j in Eq. (9) is defined in references to Eq. (1) as either μ_{F} or μ_{V} according to the process type j (gg, VBF, WH, ZH, $\text{t}\bar{\text{t}}\text{H}$, $\text{b}\bar{\text{b}}\text{H}$, $\text{q}\bar{\text{q}} \to 4\ell$, and $\text{Z} + \text{X}$). Each process includes both signal (sig) and background (bkg) components, but may contain only signal ($\text{t}\bar{\text{t}}\text{H}$ and $\text{b}\bar{\text{b}}\text{H}$) or only background ($\text{q}\bar{\text{q}} \to 4\ell$ and $\text{Z} + \text{X}$) contributions in the particular cases. The interference between the signal and background components, when both are present, is negligible in the on-shell region because of the very small width Γ_{H} compared to the mass range of interest. This also leads to the on-shell parameterization in Eq. (9) being independent from the width Γ_{H}.

The off-shell probability density follows Eqs. (1) and (9) closely but with the additional contri-

bution of interference (int) between the signal and background amplitudes as

$$\mathcal{P}_{jk}(\vec{x};\vec{\xi}_{jk},\vec{\zeta}) = \frac{\mu_j\Gamma_{\mathrm{H}}}{\Gamma_0}\,\mathcal{P}^{\mathrm{sig}}_{jk}\left(\vec{x};\vec{\xi}_{jk},f_{ai},\phi_{ai}\right) + \sqrt{\frac{\mu_j\Gamma_{\mathrm{H}}}{\Gamma_0}}\,\mathcal{P}^{\mathrm{int}}_{jk}\left(\vec{x};\vec{\xi}_{jk},f_{ai},\phi_{ai}\right) + \mathcal{P}^{\mathrm{bkg}}_{jk}\left(\vec{x};\vec{\xi}_{jk}\right), \quad (10)$$

where the notation remains the same as for Eq. (9). The $\vec{x}$ observables are listed in Table 3 and are specific to each coupling analysis. They include $m_{4\ell}$ and two other discriminants. The process type j does not include $\mathrm{t\bar{t}H}$ and $\mathrm{b\bar{b}H}$ because of their negligible contribution in the off-shell region, while the VBF, WH, and ZH processes are combined into one EW process. The parameterization in Eq. (10) depends on the width Γ_{H} explicitly and the reference value is taken to be $\Gamma_0 = 4.07\,\mathrm{MeV}$, which determines the relative strength of $\mathcal{P}^{\mathrm{sig}}_{jk}$ and $\mathcal{P}^{\mathrm{int}}_{jk}$ with respect to $\mathcal{P}^{\mathrm{bkg}}_{jk}$ in the parameterization.

The EW H boson production (VBF and VH) or production via gluon fusion have different dependence on anomalous HVV couplings, equally in the on-shell or off-shell regions. There are two HVV vertices in the former production mechanism with the subsequent $\mathrm{H} \to \mathrm{VV} \to 4\ell$ decay while there is only one HVV decay vertex in the latter case. In addition, there is interference with the background in the off-shell region. This leads to the following general expressions for the signal (sig) or interference (int) contributions appearing in Eqs. (9) and (10):

$$\mathcal{P}^{\mathrm{sig/int}}_{jk}\left(\vec{x};\vec{\xi}_{jk},f_{ai},\phi_{ai}\right) = \sum_{m=0}^{M}\mathcal{P}^{\mathrm{sig/int}}_{jk,m}\left(\vec{x};\vec{\xi}_{jk}\right) f_{ai}^{\frac{m}{2}}\,(1-f_{ai})^{\frac{M-m}{2}}\cos^m(\phi_{ai}), \quad (11)$$

where the sum over the index m runs up to $M = 4$ in the case of the EW signal process; $M = 2$ in the case of the gluon fusion, $\mathrm{t\bar{t}H}$, and $\mathrm{b\bar{b}H}$ signal processes, or the interference between the signal and background in the EW process; and $M = 1$ in the case of the interference between the signal and background in the gluon fusion process. Here, $\cos(\phi_{ai}) = \pm 1$ affects only the sign of the contributing terms.

The $\mathcal{P}^{\mathrm{sig/int}}_{jk,m}$ and $\mathcal{P}^{\mathrm{bkg}}_{jk}$ probability densities are normalized to the expected number of events, and are binned histograms (templates) of the observables $\vec{x}$ listed in Tables 2 and 3, except for the signal $m_{4\ell}$ parameterization in the on-shell region as discussed below. These templates are obtained by reweighting the existing signal or background samples for different couplings and then finding their linear combination. Since $m_{4\ell}$ is treated directly as an observable in the on-shell SM-like fit, the signal $m_{4\ell}$ shape for each process j and category k is parameterized using a double-sided Crystal-Ball function [90], and the full signal probability density is parameterized as the product of the parametric $m_{4\ell}$ shape and a template of other discriminants conditional in $m_{4\ell}$. In all cases, the H boson mass $m_{\mathrm{H}} = 125\,\mathrm{GeV}$ is assumed.

The final constraints on $f_{ai}\cos(\phi_{ai})$ and Γ_{H} are placed using the profile likelihood method using the RooFit toolkit [91] within the ROOT [92] framework. The extended likelihood function is constructed using the probability densities in Eqs. (9) and (10) with each event characterized by the discrete category k and typically three continuous observables $\vec{x}$. The likelihood $\mathcal{L}$ is maximized with respect to the nuisance parameters $\vec{\xi}_{jk}$ describing the systematic uncertainties discussed below and the yield parameters μ_{F} and μ_{V}. The allowed 68% and 95%CL intervals are defined using the profile likelihood function, $-2\Delta\ln\mathcal{L} = 1.00$ and 3.84, for which exact coverage is expected in the asymptotic limit [93].

Several systematic uncertainties are featured in the vectors of constrained parameters $\vec{\xi}_{jk}$. The template shapes describing probability distributions in Eqs. (9), (10), and (11) are varied separately within either theoretical or experimental uncertainties. In the following, a range of un-

certainties affecting the template distributions is given for the $m_{4\ell}$ values from around 100 GeV (typical for the on-shell range) to around 1 TeV (in the off-shell range), respectively. The factorization (or renormalization) scale uncertainties are evaluated by multiplying the central scale by 2 or 1/2, and the uncertainties range from $\pm0.7\%$ ($^{+1.2}_{-1.4}\%$) to $^{-1.0}_{+0.6}\%$ ($^{+5}_{-4}\%$) in the gg process, from $^{+0.6}_{-0.1}\%$ ($^{+5}_{-4}\%$) to $\pm5\%$ ($^{+30}_{-25}\%$) in the VBF processes, from $^{+3}_{-5}\%$ ($^{+5}_{-4}\%$) to $\pm6\%$ ($^{+30}_{-25}\%$) in the processes with an associated EW boson, and from $^{+3.5}_{-5.5}\%$ to $\pm1\%$ ($\pm3\%$) in the $q\bar{q} \to 4\ell$ background. PDF parameterization uncertainties are evaluated by taking the envelope of the 100 alternative NNPDF variations. Variations due to PDF parameterization uncertainties (or due to uncertainties in $\alpha_S(m_Z) = 0.1180 \pm 0.0015$) range from $^{+1.2}_{-1.4}\%$ ($^{+2.0}_{-2.5}\%$) to $^{+5}_{-4}\%$ ($^{+2.4}_{-1.0}\%$) in the gg process, from $^{+5}_{-4}\%$ to about $^{+30}_{-25}\%$ in the EW processes, and are approximately $\pm3\%$ (from $^{+1.0}_{-1.8}\%$ to $\pm0.5\%$) for the $q\bar{q} \to 4\ell$ background. The signal processes, and the backgrounds that interfere with the signal, feature the uncertainties as a function of the multiplicity and kinematics of associated jets due to the hadronization scale used in PYTHIA and the underlying event variations, obtained with the variations of the PYTHIA tune. Template shapes in the gg processes are also varied to account for a second jet in the hard process. The $q\bar{q} \to 4\ell$ background further features an uncertainty in the NLO EW corrections applied to the simulation [79, 80], which are significant at higher $m_{4\ell}$ values, up to 20% at 1 TeV.

Experimental uncertainties involve lepton efficiency and momentum uncertainties, which are similar for the different processes and categories, and jet energy calibration (JEC) uncertainties, which are only relevant when production categories are considered. The cross section uncertainties due to electron (muon) efficiency range from $^{+6}_{-7}\%$ ($^{+3.0}_{-4.5}\%$) to $^{+3.5}_{-4.5}\%$ ($^{+0.8}_{-2.0}\%$) to $^{+7}_{-8}\%$ ($^{+0.8}_{-2.0}\%$) in the 2e2μ channel, and roughly double for the 4e (4μ) channel, where the second number in the range is quoted for $m_{4\ell} \sim 230$ GeV. Systematic uncertainties in the JEC account for variations in the VBF-tagged (VH-tagged) category, and range from $\pm13\%$ ($\pm4\%$) to $\pm8\%$ ($\pm1\%$) in the gg process, from $\pm5\%$ ($^{-10}_{+2}\%$) to about $\pm11\%$ ($\pm6\%$) in the VBF process, from $\pm9\%$ ($\pm4\%$) to $\pm12\%$ ($\pm1\%$) in processes with an associated EW boson, and from $\pm17\%$ ($\pm8\%$) to $\pm15\%$ ($^{+2.0}_{-0.5}\%$) for the $q\bar{q} \to 4\ell$ background.

In the estimation of the Z + X background, the flavor composition of hadronic jets misidentified as leptons may be different in the $Z + 1\ell$ and $Z + 2\ell$ control regions, and together with the statistical uncertainty in the $Z + 2\ell$ region, this uncertainty accounts for about $\pm30\%$ variation in the background estimate from the 2017 data set. The uncertainty on the modeling of this misidentification as a function of p_T and η, combined with the $Z + 1\ell$ control region statistical uncertainty, leads to a $^{+20}_{-12}\%$ to $^{+30}_{-27}\%$ variation in the 4e channel, $\pm(10 - 20)\%$ variation in the $m_{4\ell}$ shape in the 2e2μ channel, and $\pm4\%$ to $^{+14}_{-17}\%$ variation in the 4μ channel. Uncertainties in the Z + X background in the 2016 data set are only slightly larger. The normalization of the background processes derived from the MC simulation is affected by the uncertainties in the integrated luminosity of 2.5% [94] and 2.3% [95] in the 2016 and 2017 data sets, respectively. The integrated luminosity is measured using data from the CMS silicon pixel detector, drift tubes, and the forward hadron calorimeters, or from the fast beam conditions monitor and pixel luminosity telescope. All systematic uncertainties are treated as correlated between different time periods except for the luminosity and jet-related uncertainties which originate from statistically independent sources.

As mentioned previously, the observables $\vec{x}$ used in the analysis of the data are summarized in Tables 2 and 3. The distributions of events for several of these observables are illustrated in Fig. 2 for the on-shell and in Fig. 3 for the off-shell regions. In Figs. 2 and 3, cross sections of all background processes are fixed to the SM expectations, except for the Z + X background estimated from the data control regions discussed above. Cross sections of all signal processes,

including BSM, are normalized to the SM expectations in the on-shell region.

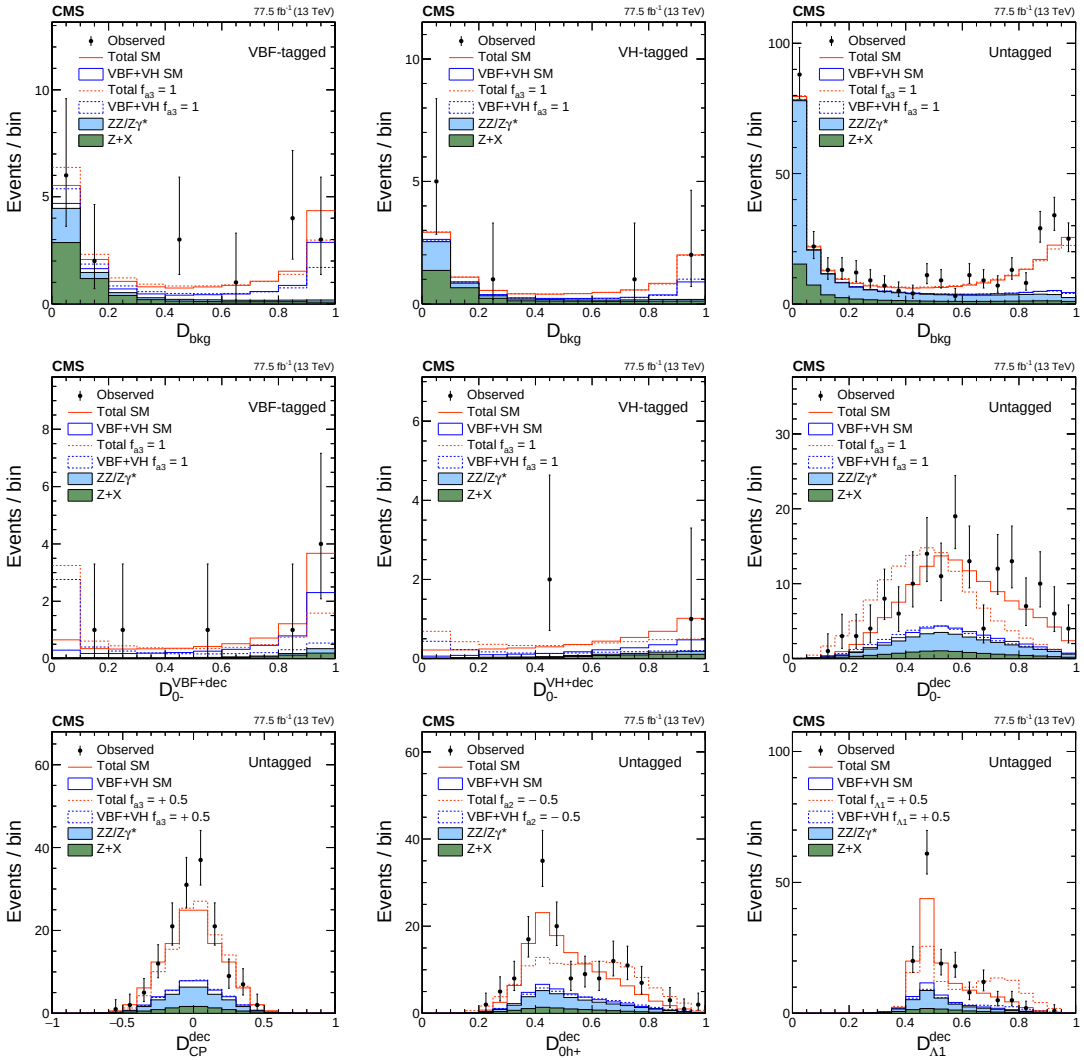

Figure 2: The distributions of events in the on-shell region in the data from 2016 and 2017. The top row shows $\mathcal{D}_{\text{bkg}}$ in the VBF-tagged (left), VH-tagged (middle), and untagged (right) categories of the analysis of the a_3 coupling for a pseudoscalar contribution. The rest of the distributions are shown with the requirement $\mathcal{D}_{\text{bkg}} > 0.5$ in order to enhance signal over background contributions. The middle row shows $\mathcal{D}_{0-}$ in the corresponding three categories. The bottom row shows $\mathcal{D}_{CP}^{\text{dec}}$ of the a_3, $\mathcal{D}_{0h+}^{\text{dec}}$ of the a_2, and $\mathcal{D}_{\Lambda 1}^{\text{dec}}$ of the Λ_1 analyses in the untagged categories.

6 Results

Four $f_{ai}\cos(\phi_{ai})$ parameters sensitive to anomalous HVV interactions, as defined in Eqs. (2) and (4), are tested in the on-shell data sample using the probability densities defined in Eq. (9). Since only the real couplings are tested, $\cos(\phi_{ai}) = \pm 1$. Figure 4 shows the results of the likelihood scans of these parameters for the 2016 and 2017 periods of the 13 TeV run and for the full combined data set from collisions at 7, 8, and 13 TeV. The analysis of the 2016 and 2017 data uses the approach presented here with the observables sensitive to anomalous couplings in both production and decay. Because of the smaller numbers of events, the data from the

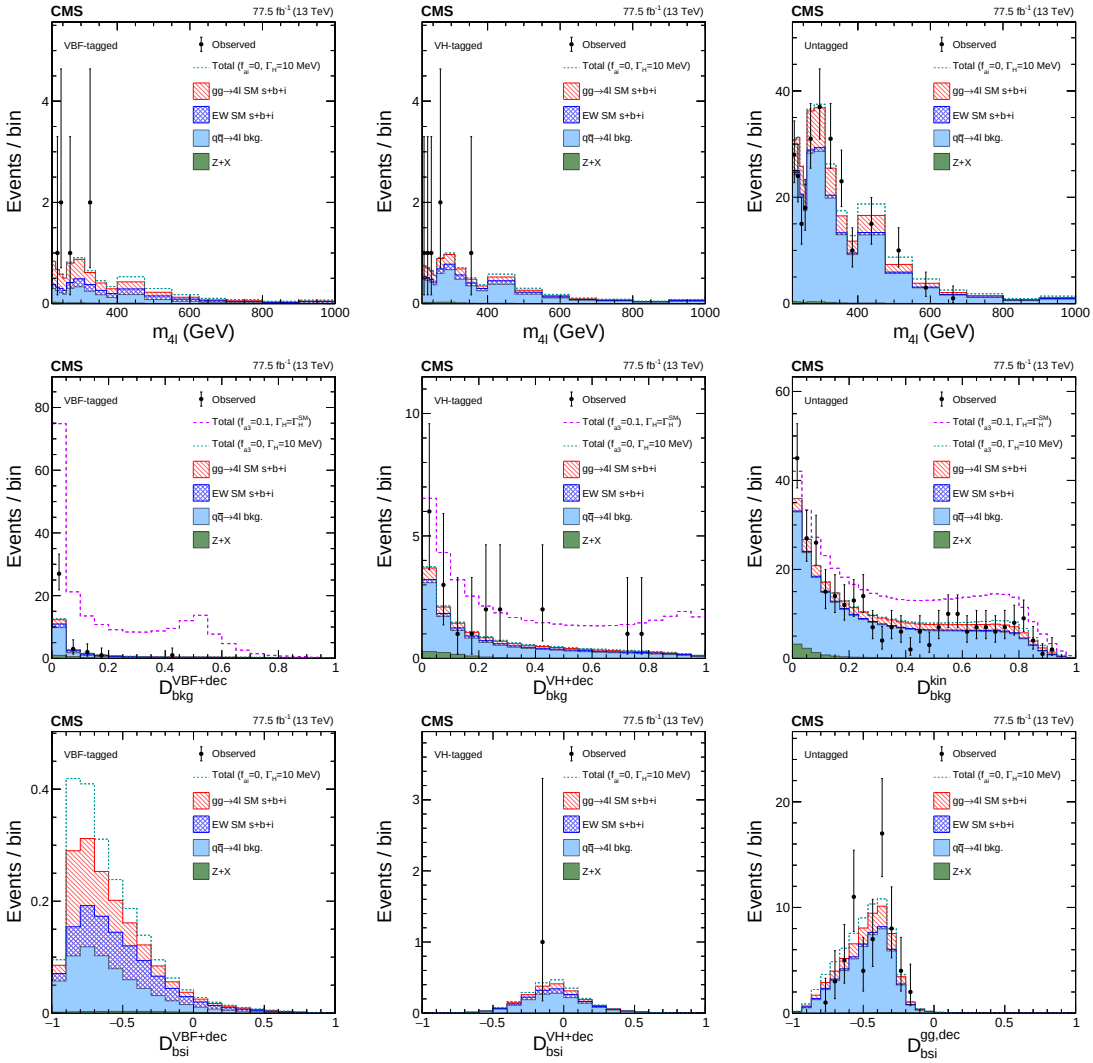

Figure 3: The distributions of events in the off-shell region in the data from 2016 and 2017. The top row shows $m_{4\ell}$ in the VBF-tagged (left), VH-tagged (middle), and untagged (right) categories in the dedicated SM-like width analysis where a requirement on $\mathcal{D}_{\text{bkg}}^{\text{VBF+dec}}$, $\mathcal{D}_{\text{bkg}}^{\text{VH+dec}}$, or $\mathcal{D}_{\text{bkg}}^{\text{kin}} > 0.6$ is applied in order to enhance signal over background contributions. The middle row shows $\mathcal{D}_{\text{bkg}}^{\text{VBF+dec}}$ (left), $\mathcal{D}_{\text{bkg}}^{\text{VH+dec}}$ (middle), $\mathcal{D}_{\text{bkg}}^{\text{kin}}$ (right) of the a_3 analysis in the corresponding three categories. The requirement $m_{4\ell} > 340\,\text{GeV}$ is applied in order to enhance signal over background contributions. The bottom row shows $\mathcal{D}_{\text{bsi}}$ in the corresponding three categories in the dedicated SM-like width analysis with both of the $m_{4\ell}$ and $\mathcal{D}_{\text{bkg}}^{\text{kin}}$ requirements enhancing the signal contribution. The acronym s + b + i designate the sum of the signal (s), background (b), and their interference contributions (i).

2015 period of the 13 TeV run and from the 2011 and 2012 periods of the 7 and 8 TeV runs are analyzed using only the decay information as in Refs. [25, 27], which is equivalent to having all events in the untagged category of this analysis. The results from on-shell events in the combined data set are listed in Table 6. These results supersede our previous measurements of these parameters in Refs. [25, 27].

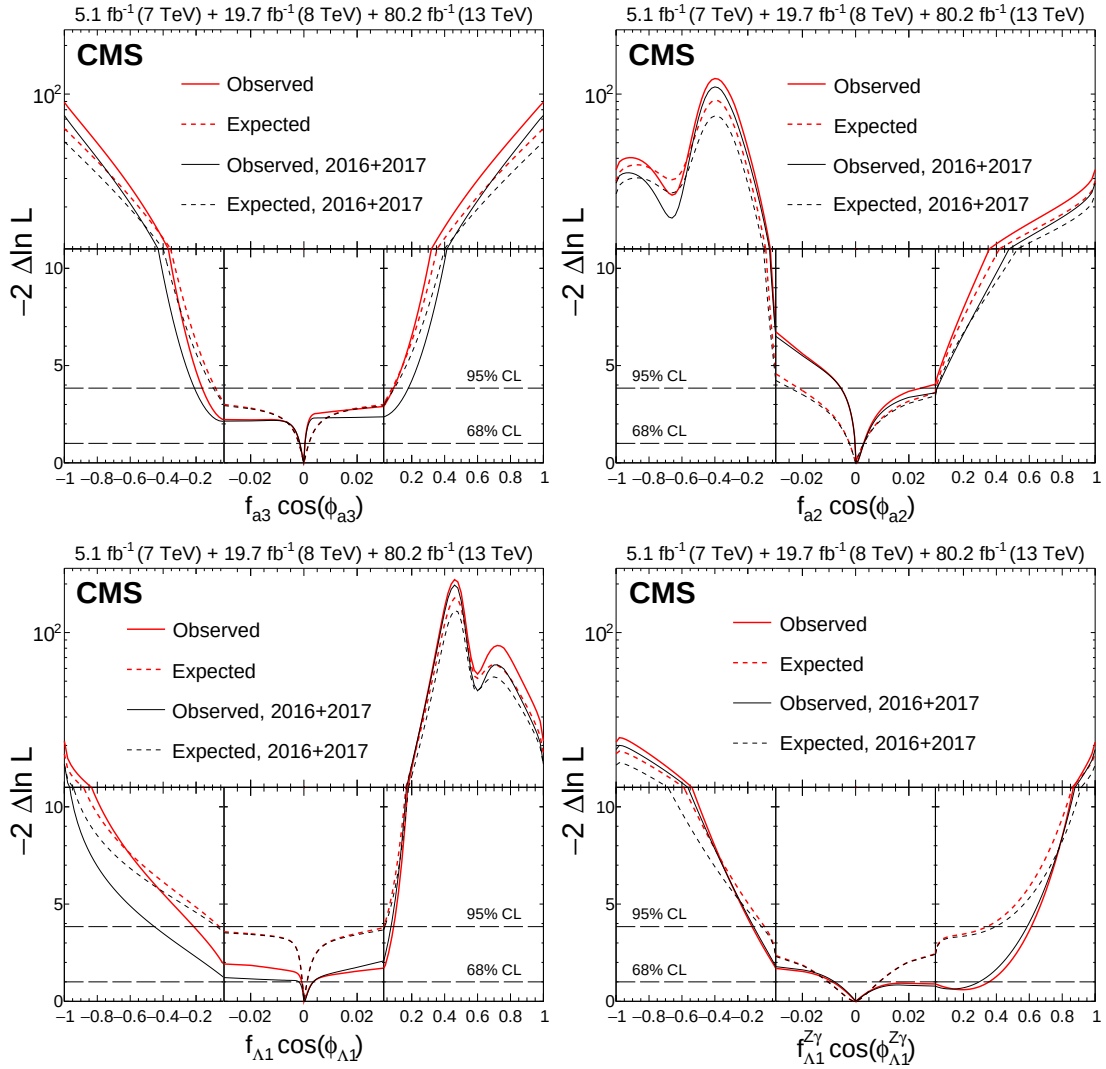

Figure 4: Observed (solid) and expected (dashed) likelihood scans of $f_{a3}\cos(\phi_{a3})$ (top-left), $f_{a2}\cos(\phi_{a2})$ (top-right), $f_{\Lambda 1}\cos(\phi_{\Lambda 1})$ (bottom-left), and $f_{\Lambda 1}^{Z\gamma}\cos\left(\phi_{\Lambda 1}^{Z\gamma}\right)$ (bottom-right) using on-shell events only. Results of analysis of the data from 2016 and 2017 only (black) and the combined Run 1 and Run 2 analysis (red) are shown. The dashed horizontal lines show the 68 and 95% CL regions.

The observed and expected 68% CL constraints are significantly tighter than in the Run 1 analysis [25] as it is evident from the narrow minima at $f_{ai} = 0$ in Fig. 4. This effect comes from utilizing production information because the cross section in VBF and VH production increases quickly with f_{ai}. Moreover, the minima of the $-2\ln\mathcal{L}$ distributions appear rather sharp because of the higher order polynomial of the f_{ai} parameters appearing in Eq. (11) in the case of VBF and VH production. At the same time, the constraints above $f_{ai} \sim 0.02$ are dominated by the decay information from $H \to 4\ell$. The best fit (μ_F, μ_V) values in the four analyses under the assumption that $f_{ai} = 0$ are as follows: $(1.21^{+0.21}_{-0.17}, 0.84^{+0.71}_{-0.59})$ at $f_{a3} = 0$, $(1.19^{+0.21}_{-0.17}, 0.91^{+0.69}_{-0.55})$ at

Table 6: Summary of allowed 68% CL (central values with uncertainties) and 95% CL (in square brackets) intervals for the anomalous coupling parameters $f_{ai}\cos(\phi_{ai})$ obtained from the analysis of the combination of Run 1 (only on-shell) and Run 2 (on-shell and off-shell) data sets. Three constraint scenarios are shown: using only on-shell events, using both on-shell and off-shell events with the Γ_H left unconstrained, or with the constraint $\Gamma_H = \Gamma_H^{SM}$.

Parameter	Scenario	Observed	Expected
$f_{a3}\cos(\phi_{a3})$	on-shell	$-0.0001^{+0.0004}_{-0.0015}$ $[-0.163, 0.090]$	$0.0000^{+0.0019}_{-0.0019}$ $[-0.082, 0.082]$
	any Γ_H	$0.0000^{+0.0003}_{-0.0010}$ $[-0.0165, 0.0087]$	$0.0000^{+0.0015}_{-0.0015}$ $[-0.038, 0.038]$
	$\Gamma_H = \Gamma_H^{SM}$	$0.0000^{+0.0003}_{-0.0009}$ $[-0.0067, 0.0050]$	$0.0000^{+0.0014}_{-0.0014}$ $[-0.0098, 0.0098]$
$f_{a2}\cos(\phi_{a2})$	on-shell	$0.0004^{+0.0026}_{-0.0006}$ $[-0.0055, 0.0234]$	$0.0000^{+0.0030}_{-0.0023}$ $[-0.021, 0.035]$
	any Γ_H	$0.0004^{+0.0026}_{-0.0006}$ $[-0.0035, 0.0147]$	$0.0000^{+0.0019}_{-0.0017}$ $[-0.015, 0.021]$
	$\Gamma_H = \Gamma_H^{SM}$	$0.0005^{+0.0025}_{-0.0006}$ $[-0.0029, 0.0129]$	$0.0000^{+0.0012}_{-0.0016}$ $[-0.010, 0.012]$
$f_{\Lambda1}\cos(\phi_{\Lambda1})$	on-shell	$0.0002^{+0.0030}_{-0.0009}$ $[-0.209, 0.089]$	$0.0000^{+0.0012}_{-0.0006}$ $[-0.059, 0.032]$
	any Γ_H	$0.0001^{+0.0015}_{-0.0006}$ $[-0.090, 0.059]$	$0.0000^{+0.0013}_{-0.0007}$ $[-0.017, 0.019]$
	$\Gamma_H = \Gamma_H^{SM}$	$0.0001^{+0.0015}_{-0.0005}$ $[-0.016, 0.068]$	$0.0000^{+0.0013}_{-0.0006}$ $[-0.015, 0.018]$
$f_{\Lambda1}^{Z\gamma}\cos\left(\phi_{\Lambda1}^{Z\gamma}\right)$	on-shell	$0.0000^{+0.3554}_{-0.0087}$ $[-0.17, 0.61]$	$0.0000^{+0.0091}_{-0.0100}$ $[-0.098, 0.343]$

Table 7: Summary of the allowed 95% CL intervals for the anomalous HVV couplings using results in Table 6. The coupling ratios are assumed to be real and include the factor $\cos(\phi_{\Lambda1})$ or $\cos\left(\phi_{\Lambda1}^{Z\gamma}\right) = \pm1$.

Parameter	Scenario	Observed	Expected
a_3/a_1	on-shell	$[-1.13, 0.80]$	$[-0.76, 0.76]$
	any Γ_H	$[-0.33, 0.24]$	$[-0.50, 0.50]$
	$\Gamma_H = \Gamma_H^{SM}$	$[-0.21, 0.18]$	$[-0.25, 0.25]$
a_2/a_1	on-shell	$[-0.12, 0.26]$	$[-0.24, 0.31]$
	any Γ_H	$[-0.098, 0.202]$	$[-0.21, 0.25]$
	$\Gamma_H = \Gamma_H^{SM}$	$[-0.089, 0.189]$	$[-0.17, 0.18]$
$(\Lambda_1\sqrt{\lvert a_1\rvert})\cos(\phi_{\Lambda1})$ (GeV)	on-shell	$[-\infty, -130] \cup [160, \infty]$	$[-\infty, -180] \cup [210, \infty]$
	any Γ_H	$[-\infty, -160] \cup [180, \infty]$	$[-\infty, -250] \cup [240, \infty]$
	$\Gamma_H = \Gamma_H^{SM}$	$[-\infty, -250] \cup [170, \infty]$	$[-\infty, -260] \cup [250, \infty]$
$(\Lambda_1^{Z\gamma}\sqrt{\lvert a_1\rvert})\cos\left(\phi_{\Lambda1}^{Z\gamma}\right)$ (GeV)	on-shell	$[-\infty, -170] \cup [100, \infty]$	$[-\infty, -200] \cup [130, \infty]$

$f_{a2} = 0$, $(1.26^{+0.20}_{-0.18}, 0.53^{+0.64}_{-0.50})$ at $f_{\Lambda1} = 0$, and $(1.24^{+0.19}_{-0.17}, 0.55^{+0.64}_{-0.51})$ at $f_{\Lambda1}^{Z\gamma} = 0$. The values obtained for the different analyses vary because of the different categorization and observables in each a_i analysis.

The combination of on-shell and off-shell regions allows the setting of tighter constraints on $f_{ai}\cos(\phi_{ai})$ using the probability densities defined in Eqs. (9) and (10). As discussed above, the on-shell region is analyzed using the 2015, 2016, and 2017 data, and the earlier Run 1 data. The off-shell region is analyzed using only 2016 and 2017 data because no such analysis of the three anomalous couplings has been performed with the Run 1 or 2015 data in this region. The one-parameter likelihood scans of $f_{ai}\cos(\phi_{ai})$ combining all such available on-shell and off-shell events is shown for two cases in Fig. 5, either with Γ_H unconstrained in the fit or with

the constraint $\Gamma_H = \Gamma_H^{SM}$. The corresponding 68 and 95% CL constraints are summarized in Table 6. The full two-parameter likelihood scans of $f_{ai}\cos(\phi_{ai})$ and Γ_H are likewise shown in Fig. 5. Using the transformation in Eq. (5), the $f_{ai}\cos(\phi_{ai})$ results can be interpreted for the coupling parameters used in Eq. (2), as shown in Table 7.

Limits on Γ_H are set by combining events from the on-shell and off-shell regions. The left hand panel of Fig. 6 shows the results of the likelihood scans of Γ_H for the 2016 and 2017 period of the 13 TeV run and for the combined data set from collisions at 7, 8 and 13 TeV under the assumption of SM-like couplings. The small contribution from the 2015 data set is not considered in this case, but the Run 1 analysis includes both the on-shell and off-shell regions in the analysis of the $H \to ZZ \to 4\ell$ decay [11, 13]. The combined results are listed in Table 8. The best fit (μ_F, μ_V) values in these results are $(1.20^{+0.19}_{-0.16}, 0.62^{+0.57}_{-0.43})$ when $\Gamma_H = \Gamma_H^{SM}$, and $(1.21^{+0.19}_{-0.17}, 0.65^{+0.61}_{-0.45})$ when Γ_H is unconstrained. The width constraints are also placed with the $f_{a3}\cos(\phi_{a3})$, $f_{a2}\cos(\phi_{a2})$, or $f_{\Lambda 1}\cos(\phi_{\Lambda 1})$ parameters unconstrained, and are shown in Fig. 6 right panel and summarized in Table 9. These results are obtained with the same fit configurations as for the study of anomalous couplings in the combination of the on-shell and off-shell regions.

Table 8: Summary of the total width Γ_H measurement, showing the allowed 68% CL (central values with uncertainties) and 95% CL (in square brackets). The limits are reported for the SM-like couplings using the Run 1 and Run 2 combination.

Parameter	Observed	Expected
Γ_H (MeV)	$3.2^{+2.8}_{-2.2}$ [0.08, 9.16]	$4.1^{+5.0}_{-4.0}$ [0.0, 13.7]

Table 9: Summary of the total width Γ_H measurements, showing allowed 68% CL (central values with uncertainties) and 95% CL (in square brackets). The Γ_H limits are reported for the anomalous coupling parameter of interest unconstrained using the Run 1 and Run 2 combination.

Parameter	Unconstrained parameter	Observed	Expected
Γ_H (MeV)	$f_{a3}\cos(\phi_{a3})$	$2.4^{+2.7}_{-1.8}$ [0.02, 8.38]	$4.1^{+5.2}_{-4.1}$ [0.0, 13.9]
Γ_H (MeV)	$f_{a2}\cos(\phi_{a2})$	$2.5^{+2.9}_{-1.8}$ [0.02, 8.76]	$4.1^{+5.2}_{-4.1}$ [0.0, 13.9]
Γ_H (MeV)	$f_{\Lambda 1}\cos(\phi_{\Lambda 1})$	$2.4^{+2.5}_{-1.6}$ [0.06, 7.84]	$4.1^{+5.2}_{-4.1}$ [0.0, 13.9]

Table 10: Summary of allowed 68% CL (central values with uncertainties) and 95% CL (in square brackets) intervals for $\mu^{\text{off-shell}}$, $\mu_F^{\text{off-shell}}$, and $\mu_V^{\text{off-shell}}$ obtained from the analysis of the combination of Run 1 and Run 2 off-shell data sets.

Parameter	Observed	Expected
$\mu^{\text{off-shell}}$	$0.78^{+0.72}_{-0.53}$ [0.02, 2.28]	$1.00^{+1.20}_{-0.99}$ [0.0, 3.2]
$\mu_F^{\text{off-shell}}$	$0.86^{+0.92}_{-0.68}$ [0.0, 2.7]	$1.0^{+1.3}_{-1.0}$ [0.0, 3.5]
$\mu_V^{\text{off-shell}}$	$0.67^{+1.26}_{-0.61}$ [0.0, 3.6]	$1.0^{+3.8}_{-1.0}$ [0.0, 8.4]

The systematic uncertainties mostly cancel in the ratios of cross sections in the measurement of fractional parameters $f_{ai}\cos(\phi_{ai})$, and are therefore negligible. The width constraints are also dominated by the statistical uncertainties, but because of the non-trivial dependence of systematic uncertainties on $m_{4\ell}$, their dominant contributions may be worth examination. The two leading theoretical and two leading experimental uncertainties affecting the width constraints (observed and expected at 68% CL) are the uncertainty on the NLO EW corrections for the $q\bar{q} \to 4\ell$ background (± 0.5 and ± 1.9 MeV), the variation of renormalization scale in gluon

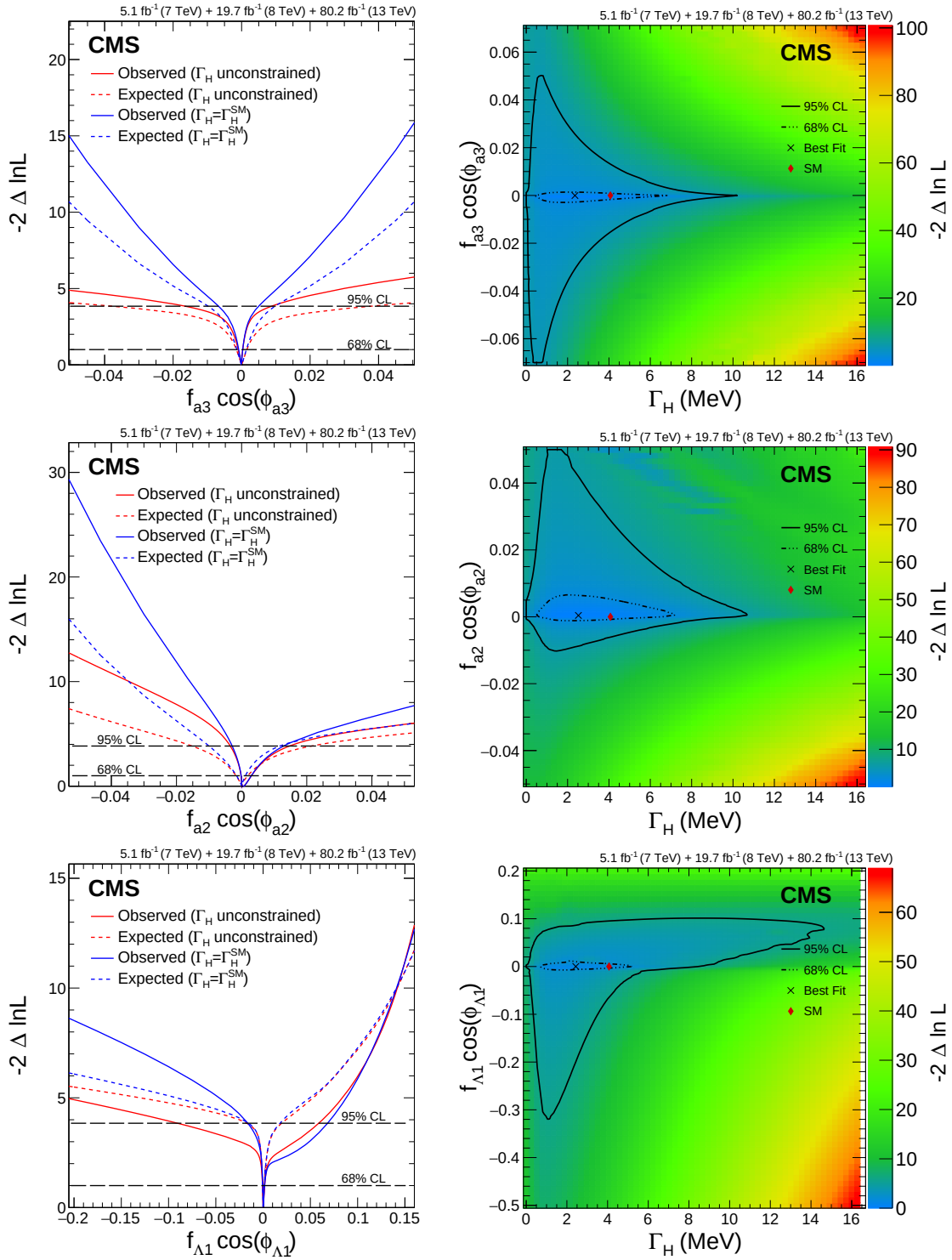

Figure 5: Constraints on $f_{a3}\cos(\phi_{a3})$ (top), $f_{a2}\cos(\phi_{a2})$ (middle), and $f_{\Lambda 1}\cos(\phi_{\Lambda 1})$ (bottom) from the combined Run 1 and Run 2 data set using both on-shell and off-shell events. Left plots: Likelihood scans of the parameters of interest with unconstrained Γ_H (red) or assuming $\Gamma_H = \Gamma_H^{SM}$ (blue). The dashed horizontal lines show the 68 and 95% CL regions. Right plots: Observed two-parameter (Γ_H, $f_{ai}\cos(\phi_{ai})$) likelihood scans. The two-parameter 68 and 95% CL regions are indicated with the dashed and solid curves, respectively.

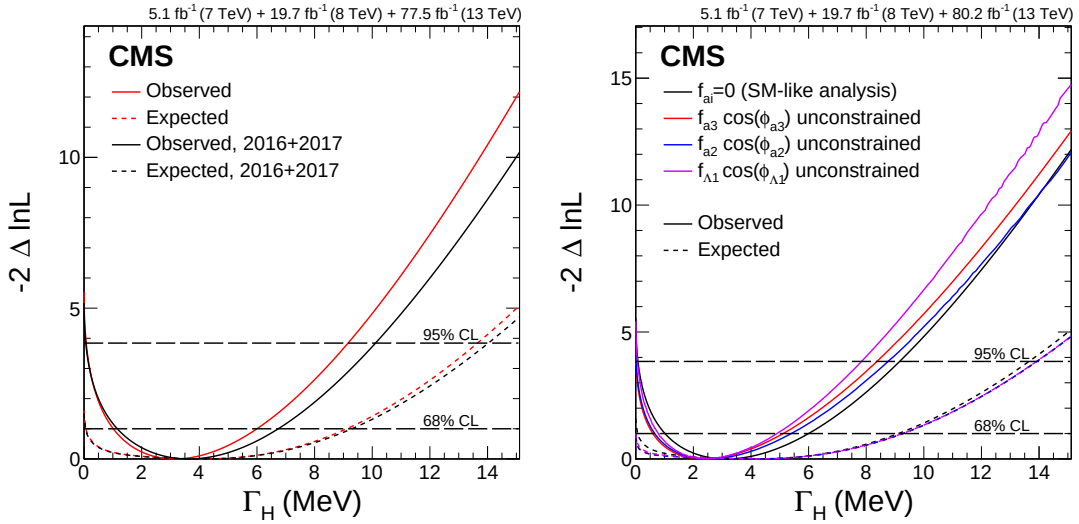

Figure 6: Observed (solid) and expected (dashed) likelihood scans of Γ_H. Left plot: Results of the SM-like couplings analysis are shown using the data only from 2016 and 2017 (black) or from the combination of Run 1 and Run 2 (red), which do not include 2015 data. Right plot: Results of the combined Run 1 and Run 2 data analyses, with 2015 data included in the on-shell case, for the SM-like couplings or with three unconstrained anomalous coupling parameters, $f_{a3}\cos(\phi_{a3})$ (red), $f_{a2}\cos(\phi_{a2})$ (blue), and $f_{\Lambda 1}\cos(\phi_{\Lambda 1})$ (violet). The dashed horizontal lines show the 68% and 95% CL regions.

fusion (± 0.2 and ± 0.4 MeV), the muon efficiency uncertainty (± 0.1 and ± 0.4 MeV), and the electron efficiency uncertainty (± 0.1 and ± 0.3 MeV).

The width constraints could also be reinterpreted as an off-shell signal strength with a change of parameters. For this interpretation, we perform an SM-like analysis of only the off-shell events, where the signal strength is modified by the parameter $\mu^{\text{off-shell}}$ common to all production mechanisms in Eqs. (1) and (10), with $\Gamma_H = \Gamma_0 = \Gamma_H^{SM}$ and the SM expectation corresponding to $\mu^{\text{off-shell}} = 1$. In addition, we also perform a fit of the off-shell events with two unconstrained parameters $\mu_F^{\text{off-shell}}$ and $\mu_V^{\text{off-shell}}$, which express the signal strengths in the gluon fusion and EW processes, respectively. These constraints are summarized in Table 10.

7 Summary

Studies of on-shell and off-shell H boson production in the four-lepton final state are presented, using data from the CMS experiment at the LHC that correspond to an integrated luminosity of 80.2 fb^{-1} at a center-of-mass energy of 13 TeV. Joint constraints are set on the H boson total width and parameters that express its anomalous couplings to two electroweak vector bosons. These results are combined with those obtained from the data collected at center-of-mass energies of 7 and 8 TeV, corresponding to integrated luminosities of 5.1 and 19.7 fb^{-1}, respectively. Kinematic information from the decay particles and the associated jets are combined using matrix element techniques to identify the production mechanism and increase sensitivity to the H boson couplings in both production and decay. The constraints on anomalous HVV couplings are found to be consistent with the standard model expectation in both on-shell and off-shell regions, as presented in Tables 6 and 7. Under the assumption of a coupling structure similar to that in the standard model, the H boson width is constrained to be $3.2^{+2.8}_{-2.2}$ MeV while the expected constraint based on simulation is $4.1^{+5.0}_{-4.0}$ MeV, as shown in Table 8. The constraints on the width remain similar with the inclusion of the tested anomalous HVV interactions and are

summarized in Table 9. The width results are also interpreted in terms of the H boson signal strength in the off-shell region in Table 10. The observed off-shell signal strength, or equivalently a non-zero value of the width, is two standard deviations away from a background-only hypothesis, which provides promise to measure H boson properties from a different direction when more data are available.

Acknowledgments

We thank Markus Schulze for optimizing the JHUGEN Monte Carlo simulation program and matrix element library for this analysis.

We congratulate our colleagues in the CERN accelerator departments for the excellent performance of the LHC and thank the technical and administrative staffs at CERN and at other CMS institutes for their contributions to the success of the CMS effort. In addition, we gratefully acknowledge the computing centers and personnel of the Worldwide LHC Computing Grid for delivering so effectively the computing infrastructure essential to our analyses. We also acknowledge the Maryland Advanced Research Computing Center (MARCC) for providing computing resources essential for this analysis. Finally, we acknowledge the enduring support for the construction and operation of the LHC and the CMS detector provided by the following funding agencies: BMBWF and FWF (Austria); FNRS and FWO (Belgium); CNPq, CAPES, FAPERJ, FAPERGS, and FAPESP (Brazil); MES (Bulgaria); CERN; CAS, MoST, and NSFC (China); COLCIENCIAS (Colombia); MSES and CSF (Croatia); RPF (Cyprus); SENESCYT (Ecuador); MoER, ERC IUT, and ERDF (Estonia); Academy of Finland, MEC, and HIP (Finland); CEA and CNRS/IN2P3 (France); BMBF, DFG, and HGF (Germany); GSRT (Greece); NKFIA (Hungary); DAE and DST (India); IPM (Iran); SFI (Ireland); INFN (Italy); MSIP and NRF (Republic of Korea); MES (Latvia); LAS (Lithuania); MOE and UM (Malaysia); BUAP, CINVESTAV, CONACYT, LNS, SEP, and UASLP-FAI (Mexico); MOS (Montenegro); MBIE (New Zealand); PAEC (Pakistan); MSHE and NSC (Poland); FCT (Portugal); JINR (Dubna); MON, RosAtom, RAS, RFBR, and NRC KI (Russia); MESTD (Serbia); SEIDI, CPAN, PCTI, and FEDER (Spain); MOSTR (Sri Lanka); Swiss Funding Agencies (Switzerland); MST (Taipei); ThEPCenter, IPST, STAR, and NSTDA (Thailand); TUBITAK and TAEK (Turkey); NASU and SFFR (Ukraine); STFC (United Kingdom); DOE and NSF (USA).

Individuals have received support from the Marie-Curie program and the European Research Council and Horizon 2020 Grant, contract No. 675440 (European Union); the Leventis Foundation; the A.P. Sloan Foundation; the Alexander von Humboldt Foundation; the Belgian Federal Science Policy Office; the Fonds pour la Formation à la Recherche dans l'Industrie et dans l'Agriculture (FRIA-Belgium); the Agentschap voor Innovatie door Wetenschap en Technologie (IWT-Belgium); the F.R.S.-FNRS and FWO (Belgium) under the "Excellence of Science – EOS" – be.h project n. 30820817; the Ministry of Education, Youth and Sports (MEYS) of the Czech Republic; the Lendület ("Momentum") Program and the János Bolyai Research Scholarship of the Hungarian Academy of Sciences, the New National Excellence Program ÚNKP, the NKFIA research grants 123842, 123959, 124845, 124850, and 125105 (Hungary); the Council of Science and Industrial Research, India; the HOMING PLUS program of the Foundation for Polish Science, cofinanced from European Union, Regional Development Fund, the Mobility Plus program of the Ministry of Science and Higher Education, the National Science Center (Poland), contracts Harmonia 2014/14/M/ST2/00428, Opus 2014/13/B/ST2/02543, 2014/15/B/ST2/03998, and 2015/19/B/ST2/02861, Sonata-bis 2012/07/E/ST2/01406; the National Priorities Research Program by Qatar National Research Fund; the Programa Estatal de Fomento de la Investigación Científica y Técnica de Excelencia María de Maeztu, grant MDM-2015-0509 and the Pro-

grama Severo Ochoa del Principado de Asturias; the Thalis and Aristeia programs cofinanced by EU-ESF and the Greek NSRF; the Rachadapisek Sompot Fund for Postdoctoral Fellowship, Chulalongkorn University and the Chulalongkorn Academic into Its 2nd Century Project Advancement Project (Thailand); the Welch Foundation, contract C-1845; and the Weston Havens Foundation (USA).

References

[1] S. L. Glashow, "Partial-symmetries of weak interactions", *Nucl. Phys.* **22** (1961) 579, doi:10.1016/0029-5582(61)90469-2.

[2] F. Englert and R. Brout, "Broken symmetry and the mass of gauge vector mesons", *Phys. Rev. Lett.* **13** (1964) 321, doi:10.1103/PhysRevLett.13.321.

[3] P. W. Higgs, "Broken symmetries, massless particles and gauge fields", *Phys. Lett.* **12** (1964) 132, doi:10.1016/0031-9163(64)91136-9.

[4] P. W. Higgs, "Broken symmetries and the masses of gauge bosons", *Phys. Rev. Lett.* **13** (1964) 508, doi:10.1103/PhysRevLett.13.508.

[5] G. S. Guralnik, C. R. Hagen, and T. W. B. Kibble, "Global conservation laws and massless particles", *Phys. Rev. Lett.* **13** (1964) 585, doi:10.1103/PhysRevLett.13.585.

[6] S. Weinberg, "A model of leptons", *Phys. Rev. Lett.* **19** (1967) 1264, doi:10.1103/PhysRevLett.19.1264.

[7] A. Salam, "Weak and electromagnetic interactions", in *Elementary particle physics: relativistic groups and analyticity*, N. Svartholm, ed., p. 367. Almqvist & Wiksell, Stockholm, 1968. Proceedings of the eighth Nobel symposium.

[8] ATLAS Collaboration, "Observation of a new particle in the search for the Standard Model Higgs boson with the ATLAS detector at the LHC", *Phys. Lett. B* **716** (2012) 1, doi:10.1016/j.physletb.2012.08.020, arXiv:1207.7214.

[9] CMS Collaboration, "Observation of a new boson at a mass of 125 GeV with the CMS experiment at the LHC", *Phys. Lett. B* **716** (2012) 30, doi:10.1016/j.physletb.2012.08.021, arXiv:1207.7235.

[10] CMS Collaboration, "Observation of a new boson with mass near 125 GeV in pp collisions at $\sqrt{s} = 7$ and 8 TeV", *JHEP* **06** (2013) 081, doi:10.1007/JHEP06(2013)081, arXiv:1303.4571.

[11] CMS Collaboration, "Constraints on the Higgs boson width from off-shell production and decay to Z-boson pairs", *Phys. Lett. B* **736** (2014) 64, doi:10.1016/j.physletb.2014.06.077, arXiv:1405.3455.

[12] ATLAS Collaboration, "Constraints on the off-shell Higgs boson signal strength in the high-mass ZZ and WW final states with the ATLAS detector", *Eur. Phys. J. C* **75** (2015) 335, doi:10.1140/epjc/s10052-015-3542-2, arXiv:1503.01060.

[13] CMS Collaboration, "Limits on the Higgs boson lifetime and width from its decay to four charged leptons", *Phys. Rev. D* **92** (2015) 072010, doi:10.1103/PhysRevD.92.072010, arXiv:1507.06656.

[14] CMS Collaboration, "Search for Higgs boson off-shell production in proton-proton collisions at 7 and 8 TeV and derivation of constraints on its total decay width", *JHEP* **09** (2016) 051, doi:10.1007/JHEP09(2016)051, arXiv:1605.02329.

[15] ATLAS Collaboration, "Constraints on off-shell Higgs boson production and the Higgs boson total width in ZZ $\to 4\ell$ and ZZ $\to 2\ell 2\nu$ final states with the ATLAS detector", *Phys. Lett. B* **786** (2018) 223, doi:10.1016/j.physletb.2018.09.048, arXiv:1808.01191.

[16] F. Caola and K. Melnikov, "Constraining the Higgs boson width with ZZ production at the LHC", *Phys. Rev. D* **88** (2013) 054024, doi:10.1103/PhysRevD.88.054024, arXiv:1307.4935.

[17] N. Kauer and G. Passarino, "Inadequacy of zero-width approximation for a light Higgs boson signal", *JHEP* **08** (2012) 116, doi:10.1007/JHEP08(2012)116, arXiv:1206.4803.

[18] J. M. Campbell, R. K. Ellis, and C. Williams, "Bounding the Higgs width at the LHC using full analytic results for gg $\to e^- e^+ \mu^- \mu^+$", *JHEP* **04** (2014) 060, doi:10.1007/JHEP04(2014)060, arXiv:1311.3589.

[19] CMS Collaboration, "Precise determination of the mass of the Higgs boson and tests of compatibility of its couplings with the standard model predictions using proton collisions at 7 and 8 TeV", *Eur. Phys. J. C* **75** (2015) 212, doi:10.1140/epjc/s10052-015-3351-7, arXiv:1412.8662.

[20] ATLAS Collaboration, "Measurement of the Higgs boson mass from the H $\to \gamma\gamma$ and H $\to$ ZZ$^* \to 4\ell$ channels with the ATLAS detector using 25 fb^{-1} of pp collision data", *Phys. Rev. D* **90** (2014) 052004, doi:10.1103/PhysRevD.90.052004, arXiv:1406.3827.

[21] CMS Collaboration, "Measurements of properties of the Higgs boson decaying into the four-lepton final state in pp collisions at $\sqrt{s} = 13$ TeV", *JHEP* **11** (2017) 047, doi:10.1007/JHEP11(2017)047, arXiv:1706.09936.

[22] D. de Florian et al., "Handbook of LHC Higgs cross sections: 4. deciphering the nature of the Higgs sector", CERN Report CERN-2017-002-M, 2016. doi:10.23731/CYRM-2017-002, arXiv:1610.07922.

[23] CMS Collaboration, "On the mass and spin-parity of the Higgs boson candidate via its decays to Z boson pairs", *Phys. Rev. Lett.* **110** (2013) 081803, doi:10.1103/PhysRevLett.110.081803, arXiv:1212.6639.

[24] CMS Collaboration, "Measurement of the properties of a Higgs boson in the four-lepton final state", *Phys. Rev. D* **89** (2014) 092007, doi:10.1103/PhysRevD.89.092007, arXiv:1312.5353.

[25] CMS Collaboration, "Constraints on the spin-parity and anomalous HVV couplings of the Higgs boson in proton collisions at 7 and 8 TeV", *Phys. Rev. D* **92** (2015) 012004, doi:10.1103/PhysRevD.92.012004, arXiv:1411.3441.

[26] CMS Collaboration, "Combined search for anomalous pseudoscalar HVV couplings in VH (H $\to b\bar{b}$) production and H $\to$ VV decay", *Phys. Lett. B* **759** (2016) 672, doi:10.1016/j.physletb.2016.06.004, arXiv:1602.04305.

[27] CMS Collaboration, "Constraints on anomalous Higgs boson couplings using production and decay information in the four-lepton final state", *Phys. Lett. B* **775** (2017) 1, doi:10.1016/j.physletb.2017.10.021, arXiv:1707.00541.

[28] ATLAS Collaboration, "Evidence for the spin-0 nature of the Higgs boson using ATLAS data", *Phys. Lett. B* **726** (2013) 120, doi:10.1016/j.physletb.2013.08.026, arXiv:1307.1432.

[29] ATLAS Collaboration, "Study of the spin and parity of the Higgs boson in diboson decays with the ATLAS detector", *Eur. Phys. J. C* **75** (2015) 476, doi:10.1140/epjc/s10052-015-3685-1, arXiv:1506.05669.

[30] ATLAS Collaboration, "Test of CP Invariance in vector-boson fusion production of the Higgs boson using the Optimal Observable method in the ditau decay channel with the ATLAS detector", *Eur. Phys. J. C* **76** (2016) 658, doi:10.1140/epjc/s10052-016-4499-5, arXiv:1602.04516.

[31] ATLAS Collaboration, "Measurement of inclusive and differential cross sections in the $H \to ZZ^* \to 4\ell$ decay channel in pp collisions at $\sqrt{s} = 13$ TeV with the ATLAS detector", *JHEP* **10** (2017) 132, doi:10.1007/JHEP10(2017)132, arXiv:1708.02810.

[32] ATLAS Collaboration, "Measurement of the Higgs boson coupling properties in the $H \to ZZ^* \to 4\ell$ decay channel at $\sqrt{s}$ = 13 TeV with the ATLAS detector", *JHEP* **03** (2018) 095, doi:10.1007/JHEP03(2018)095, arXiv:1712.02304.

[33] ATLAS Collaboration, "Measurements of Higgs boson properties in the diphoton decay channel with 36 fb^{-1} of pp collision data at $\sqrt{s} = 13$ TeV with the ATLAS detector", *Phys. Rev. D* **98** (2018) 052005, doi:10.1103/PhysRevD.98.052005, arXiv:1802.04146.

[34] J. S. Gainer et al., "Beyond geolocating: Constraining higher dimensional operators in $H \to 4\ell$ with off-shell production and more", *Phys. Rev. D* **91** (2015) 035011, doi:10.1103/PhysRevD.91.035011, arXiv:1403.4951.

[35] C. Englert and M. Spannowsky, "Limitations and opportunities of off-shell coupling measurements", *Phys. Rev. D* **90** (2014) 053003, doi:10.1103/PhysRevD.90.053003, arXiv:1405.0285.

[36] M. Ghezzi, G. Passarino, and S. Uccirati, "Bounding the Higgs width using effective field theory", in *Proceedings, 12th DESY Workshop on Elementary Particle Physics: Loops and Legs in Quantum Field Theory (LL2014)*, p. 072. Weimar, Germany, April, 2014. arXiv:1405.1925. [PoS(LL2014)072]. doi:10.22323/1.211.0072.

[37] CMS Collaboration, "Search for a new scalar resonance decaying to a pair of Z bosons in proton-proton collisions at $\sqrt{s} = 13$ TeV", *JHEP* **06** (2018) 127, doi:10.1007/JHEP06(2018)127, arXiv:1804.01939.

[38] C. A. Nelson, "Correlation between decay planes in Higgs-boson decays into a W Pair (into a Z Pair)", *Phys. Rev. D* **37** (1988) 1220, doi:10.1103/PhysRevD.37.1220.

[39] A. Soni and R. M. Xu, "Probing CP violation via Higgs decays to four leptons", *Phys. Rev. D* **48** (1993) 5259, doi:10.1103/PhysRevD.48.5259, arXiv:hep-ph/9301225.

[40] T. Plehn, D. L. Rainwater, and D. Zeppenfeld, "Determining the structure of Higgs couplings at the LHC", *Phys. Rev. Lett.* **88** (2002) 051801, doi:10.1103/PhysRevLett.88.051801, arXiv:hep-ph/0105325.

[41] S. Y. Choi, D. J. Miller, M. M. Mühlleitner, and P. M. Zerwas, "Identifying the Higgs spin and parity in decays to Z pairs", *Phys. Lett. B* **553** (2003) 61, doi:10.1016/S0370-2693(02)03191-X, arXiv:hep-ph/0210077.

[42] C. P. Buszello, I. Fleck, P. Marquard, and J. J. van der Bij, "Prospective analysis of spin- and CP-sensitive variables in $H \to ZZ \to \ell_1^+\ell_1^-\ell_2^+\ell_2^-$ at the LHC", *Eur. Phys. J. C* **32** (2004) 209, doi:10.1140/epjc/s2003-01392-0, arXiv:hep-ph/0212396.

[43] V. Hankele, G. Klamke, D. Zeppenfeld, and T. Figy, "Anomalous Higgs boson couplings in vector boson fusion at the CERN LHC", *Phys. Rev. D* **74** (2006) 095001, doi:10.1103/PhysRevD.74.095001, arXiv:hep-ph/0609075.

[44] E. Accomando et al., "Workshop on CP studies and non-standard Higgs physics", (2006). arXiv:hep-ph/0608079.

[45] R. M. Godbole, D. J. Miller, and M. M. Mühlleitner, "Aspects of CP violation in the HZZ coupling at the LHC", *JHEP* **12** (2007) 031, doi:10.1088/1126-6708/2007/12/031, arXiv:0708.0458.

[46] K. Hagiwara, Q. Li, and K. Mawatari, "Jet angular correlation in vector-boson fusion processes at hadron colliders", *JHEP* **07** (2009) 101, doi:10.1088/1126-6708/2009/07/101, arXiv:0905.4314.

[47] Y. Gao et al., "Spin determination of single-produced resonances at hadron colliders", *Phys. Rev. D* **81** (2010) 075022, doi:10.1103/PhysRevD.81.075022, arXiv:1001.3396.

[48] A. De Rújula et al., "Higgs look-alikes at the LHC", *Phys. Rev. D* **82** (2010) 013003, doi:10.1103/PhysRevD.82.013003, arXiv:1001.5300.

[49] N. D. Christensen, T. Han, and Y. Li, "Testing CP Violation in ZZH Interactions at the LHC", *Phys. Lett. B* **693** (2010) 28, doi:10.1016/j.physletb.2010.08.008, arXiv:1005.5393.

[50] S. Bolognesi et al., "Spin and parity of a single-produced resonance at the LHC", *Phys. Rev. D* **86** (2012) 095031, doi:10.1103/PhysRevD.86.095031, arXiv:1208.4018.

[51] J. Ellis, D. S. Hwang, V. Sanz, and T. You, "A fast track towards the 'Higgs' spin and parity", *JHEP* **11** (2012) 134, doi:10.1007/JHEP11(2012)134, arXiv:1208.6002.

[52] Y. Chen, N. Tran, and R. Vega-Morales, "Scrutinizing the Higgs signal and background in the 2e2μ golden channel", *JHEP* **01** (2013) 182, doi:10.1007/JHEP01(2013)182, arXiv:1211.1959.

[53] P. Artoisenet et al., "A framework for Higgs characterisation", *JHEP* **11** (2013) 043, doi:10.1007/JHEP11(2013)043, arXiv:1306.6464.

[54] I. Anderson et al., "Constraining anomalous HVV interactions at proton and lepton colliders", *Phys. Rev. D* **89** (2014) 035007, doi:10.1103/PhysRevD.89.035007, arXiv:1309.4819.

[55] M. Chen et al., "Role of interference in unraveling the ZZ couplings of the newly discovered boson at the LHC", *Phys. Rev. D* **89** (2014) 034002, doi:10.1103/PhysRevD.89.034002, arXiv:1310.1397.

[56] M. J. Dolan, P. Harris, M. Jankowiak, and M. Spannowsky, "Constraining *CP*-violating Higgs sectors at the LHC using gluon fusion", *Phys. Rev. D* **90** (2014) 073008, doi:10.1103/PhysRevD.90.073008, arXiv:1406.3322.

[57] M. Gonzalez-Alonso, A. Greljo, G. Isidori, and D. Marzocca, "Pseudo-observables in Higgs decays", *Eur. Phys. J. C* **75** (2015) 128, doi:10.1140/epjc/s10052-015-3345-5, arXiv:1412.6038.

[58] A. Greljo, G. Isidori, J. M. Lindert, and D. Marzocca, "Pseudo-observables in electroweak Higgs production", *Eur. Phys. J. C* **76** (2016) 158, doi:10.1140/epjc/s10052-016-4000-5, arXiv:1512.06135.

[59] A. V. Gritsan, R. Röntsch, M. Schulze, and M. Xiao, "Constraining anomalous Higgs boson couplings to the heavy flavor fermions using matrix element techniques", *Phys. Rev. D* **94** (2016) 055023, doi:10.1103/PhysRevD.94.055023, arXiv:1606.03107.

[60] CMS Collaboration, "The CMS experiment at the CERN LHC", *JINST* **3** (2008) S08004, doi:10.1088/1748-0221/3/08/S08004.

[61] S. Frixione, P. Nason, and C. Oleari, "Matching NLO QCD computations with parton shower simulations: the POWHEG method", *JHEP* **11** (2007) 070, doi:10.1088/1126-6708/2007/11/070, arXiv:0709.2092.

[62] E. Bagnaschi, G. Degrassi, P. Slavich, and A. Vicini, "Higgs production via gluon fusion in the POWHEG approach in the SM and in the MSSM", *JHEP* **02** (2012) 088, doi:10.1007/JHEP02(2012)088, arXiv:1111.2854.

[63] P. Nason and C. Oleari, "NLO Higgs boson production via vector-boson fusion matched with shower in POWHEG", *JHEP* **02** (2010) 037, doi:10.1007/JHEP02(2010)037, arXiv:0911.5299.

[64] G. Luisoni, P. Nason, C. Oleari, and F. Tramontano, "$HW^{\pm}$/HZ + 0 and 1 jet at NLO with the POWHEG BOX interfaced to GoSam and their merging within MiNLO", *JHEP* **10** (2013) 083, doi:10.1007/JHEP10(2013)083, arXiv:1306.2542.

[65] H. B. Hartanto, B. Jager, L. Reina, and D. Wackeroth, "Higgs boson production in association with top quarks in the POWHEG BOX", *Phys. Rev. D* **91** (2015) 094003, doi:10.1103/PhysRevD.91.094003, arXiv:1501.04498.

[66] K. Hamilton, P. Nason, and G. Zanderighi, "MINLO: multi-scale i mproved NLO", *JHEP* **10** (2012) 155, doi:10.1007/JHEP10(2012)155, arXiv:1206.3572.

[67] J. M. Campbell and R. K. Ellis, "MCFM for the Tevatron and the LHC", *Nucl. Phys. Proc. Suppl.* **205-206** (2010) 10, doi:10.1016/j.nuclphysbps.2010.08.011, arXiv:1007.3492.

[68] J. M. Campbell, R. K. Ellis, and C. Williams, "Vector boson pair production at the LHC", *JHEP* **07** (2011) 018, doi:10.1007/JHEP07(2011)018, arXiv:1105.0020.

[69] J. M. Campbell and R. K. Ellis, "Higgs constraints from vector boson fusion and scattering", *JHEP* **04** (2015) 030, doi:10.1007/JHEP04(2015)030, arXiv:1502.02990.

[70] A. Ballestrero et al., "PHANTOM: a Monte Carlo event generator for six parton final states at high energy colliders", *Comput. Phys. Commun.* **180** (2009) 401, doi:10.1016/j.cpc.2008.10.005, arXiv:0801.3359.

[71] S. Catani and M. Grazzini, "An NNLO subtraction formalism in hadron collisions and its application to Higgs boson production at the LHC", *Phys. Rev. Lett.* **98** (2007) 222002, doi:10.1103/PhysRevLett.98.222002, arXiv:hep-ph/0703012.

[72] M. Grazzini, "NNLO predictions for the Higgs boson signal in the H $\to$ WW $\to \ell\nu\ell\nu$ and H $\to$ ZZ $\to 4\ell$ decay channels", *JHEP* **02** (2008) 043, doi:10.1088/1126-6708/2008/02/043, arXiv:0801.3232.

[73] M. Grazzini and H. Sargsyan, "Heavy-quark mass effects in Higgs boson production at the LHC", *JHEP* **09** (2013) 129, doi:10.1007/JHEP09(2013)129, arXiv:1306.4581.

[74] F. Caola, K. Melnikov, R. Röntsch, and L. Tancredi, "QCD corrections to ZZ production in gluon fusion at the LHC", *Phys. Rev. D* **92** (2015) 094028, doi:10.1103/PhysRevD.92.094028, arXiv:1509.06734.

[75] K. Melnikov and M. Dowling, "Production of two Z-bosons in gluon fusion in the heavy top quark approximation", *Phys. Lett. B* **744** (2015) 43, doi:10.1016/j.physletb.2015.03.030, arXiv:1503.01274.

[76] J. M. Campbell, R. K. Ellis, M. Czakon, and S. Kirchner, "Two loop correction to interference in gg $\to$ ZZ", *JHEP* **08** (2016) 011, doi:10.1007/JHEP08(2016)011, arXiv:1605.01380.

[77] F. Caola et al., "QCD corrections to vector boson pair production in gluon fusion including interference effects with off-shell Higgs at the LHC", *JHEP* **07** (2016) 087, doi:10.1007/JHEP07(2016)087, arXiv:1605.04610.

[78] M. Grazzini, S. Kallweit, and D. Rathlev, "ZZ production at the LHC: fiducial cross sections and distributions in NNLO QCD", *Phys. Lett. B* **750** (2015) 407, doi:10.1016/j.physletb.2015.09.055, arXiv:1507.06257.

[79] S. Gieseke, T. Kasprzik, and J. H. Kuehn, "Vector-boson pair production and electroweak corrections in HERWIG++", *Eur. Phys. J. C* **74** (2014) 2988, doi:10.1140/epjc/s10052-014-2988-y, arXiv:1401.3964.

[80] J. Baglio, L. D. Ninh, and M. M. Weber, "Massive gauge boson pair production at the LHC: a next-to-leading order story", *Phys. Rev. D* **88** (2013) 113005, doi:10.1103/PhysRevD.88.113005, arXiv:1307.4331. [Erratum: doi:10.1103/PhysRevD.94.099902].

[81] NNPDF Collaboration, "Unbiased global determination of parton distributions and their uncertainties at NNLO and at LO", *Nucl. Phys. B* **855** (2012) 153, doi:10.1016/j.nuclphysb.2011.09.024, arXiv:1107.2652.

[82] T. Sjöstrand et al., "An introduction to PYTHIA 8.2", *Comput. Phys. Commun.* **191** (2015) 159, doi:10.1016/j.cpc.2015.01.024, arXiv:1410.3012.

[83] GEANT4 Collaboration, "GEANT4 – a simulation toolkit", *Nucl. Instrum. Meth. A* **506** (2003) 250, doi:10.1016/S0168-9002(03)01368-8.

[84] CMS Collaboration, "Particle-flow reconstruction and global event description with the cms detector", *JINST* **12** (2017) P10003, doi:10.1088/1748-0221/12/10/P10003, arXiv:1706.04965.

[85] M. Cacciari, G. P. Salam, and G. Soyez, "The anti-k_{T} jet clustering algorithm", *JHEP* **04** (2008) 063, doi:10.1088/1126-6708/2008/04/063, arXiv:0802.1189.

[86] M. Cacciari, G. P. Salam, and G. Soyez, "FastJet user manual", *Eur. Phys. J. C* **72** (2012) 1896, doi:10.1140/epjc/s10052-012-1896-2, arXiv:1111.6097.

[87] CMS Collaboration, "Identification of b-quark jets with the CMS experiment", *JINST* **8** (2013) P04013, doi:10.1088/1748-0221/8/04/P04013, arXiv:1211.4462.

[88] CMS Collaboration, "Identification of heavy-flavour jets with the CMS detector in pp collisions at 13 TeV", *JINST* **13** (2018) P05011, doi:10.1088/1748-0221/13/05/P05011, arXiv:1712.07158.

[89] R. J. Barlow, "Extended maximum likelihood", *Nucl. Instrum. Meth. A* **297** (1990) 496, doi:10.1016/0168-9002(90)91334-8.

[90] M. Oreglia, "A study of the reactions $\psi' \to \gamma\gamma\psi$". PhD thesis, Stanford University, 1980. SLAC Report SLAC-R-236.

[91] W. Verkerke and D. P. Kirkby, "The RooFit toolkit for data modeling", in *13^{th} International Conference for Computing in High-Energy and Nuclear Physics (CHEP03)*. 2003. arXiv:physics/0306116. CHEP-2003-MOLT007.

[92] R. Brun and F. Rademakers, "ROOT: An object oriented data analysis framework", *Nucl. Instrum. Meth. A* **389** (1997) 81, doi:10.1016/S0168-9002(97)00048-X.

[93] S. S. Wilks, "The large-sample distribution of the likelihood ratio for testing composite hypotheses", *Annals Math. Statist.* **9** (1938) 60, doi:10.1214/aoms/1177732360.

[94] CMS Collaboration, "CMS luminosity measurements for the 2016 data taking period", CMS Physics Analysis Summary CMS-PAS-LUM-17-001, 2017.

[95] CMS Collaboration, "CMS luminosity measurement for the 2017 data taking period at $\sqrt{s} = 13\,\mathrm{TeV}$", CMS Physics Analysis Summary CMS-PAS-LUM-17-004, 2018.

A The CMS Collaboration

Yerevan Physics Institute, Yerevan, Armenia
A.M. Sirunyan, A. Tumasyan

Institut für Hochenergiephysik, Wien, Austria
W. Adam, F. Ambrogi, E. Asilar, T. Bergauer, J. Brandstetter, M. Dragicevic, J. Erö, A. Escalante Del Valle, M. Flechl, R. Frühwirth[1], V.M. Ghete, J. Hrubec, M. Jeitler[1], N. Krammer, I. Krätschmer, D. Liko, T. Madlener, I. Mikulec, N. Rad, H. Rohringer, J. Schieck[1], R. Schöfbeck, M. Spanring, D. Spitzbart, W. Waltenberger, J. Wittmann, C.-E. Wulz[1], M. Zarucki

Institute for Nuclear Problems, Minsk, Belarus
V. Chekhovsky, V. Mossolov, J. Suarez Gonzalez

Universiteit Antwerpen, Antwerpen, Belgium
E.A. De Wolf, D. Di Croce, X. Janssen, J. Lauwers, A. Lelek, M. Pieters, H. Van Haevermaet, P. Van Mechelen, N. Van Remortel

Vrije Universiteit Brussel, Brussel, Belgium
S. Abu Zeid, F. Blekman, J. D'Hondt, J. De Clercq, K. Deroover, G. Flouris, D. Lontkovskyi, S. Lowette, I. Marchesini, S. Moortgat, L. Moreels, Q. Python, K. Skovpen, S. Tavernier, W. Van Doninck, P. Van Mulders, I. Van Parijs

Université Libre de Bruxelles, Bruxelles, Belgium
D. Beghin, B. Bilin, H. Brun, B. Clerbaux, G. De Lentdecker, H. Delannoy, B. Dorney, G. Fasanella, L. Favart, A. Grebenyuk, A.K. Kalsi, T. Lenzi, J. Luetic, N. Postiau, E. Starling, L. Thomas, C. Vander Velde, P. Vanlaer, D. Vannerom, Q. Wang

Ghent University, Ghent, Belgium
T. Cornelis, D. Dobur, A. Fagot, M. Gul, I. Khvastunov[2], D. Poyraz, C. Roskas, D. Trocino, M. Tytgat, W. Verbeke, B. Vermassen, M. Vit, N. Zaganidis

Université Catholique de Louvain, Louvain-la-Neuve, Belgium
H. Bakhshiansohi, O. Bondu, G. Bruno, C. Caputo, P. David, C. Delaere, M. Delcourt, A. Giammanco, G. Krintiras, V. Lemaitre, A. Magitteri, K. Piotrzkowski, A. Saggio, M. Vidal Marono, P. Vischia, J. Zobec

Centro Brasileiro de Pesquisas Fisicas, Rio de Janeiro, Brazil
F.L. Alves, G.A. Alves, G. Correia Silva, C. Hensel, A. Moraes, M.E. Pol, P. Rebello Teles

Universidade do Estado do Rio de Janeiro, Rio de Janeiro, Brazil
E. Belchior Batista Das Chagas, W. Carvalho, J. Chinellato[3], E. Coelho, E.M. Da Costa, G.G. Da Silveira[4], D. De Jesus Damiao, C. De Oliveira Martins, S. Fonseca De Souza, H. Malbouisson, D. Matos Figueiredo, M. Melo De Almeida, C. Mora Herrera, L. Mundim, H. Nogima, W.L. Prado Da Silva, L.J. Sanchez Rosas, A. Santoro, A. Sznajder, M. Thiel, E.J. Tonelli Manganote[3], F. Torres Da Silva De Araujo, A. Vilela Pereira

Universidade Estadual Paulista [a], Universidade Federal do ABC [b], São Paulo, Brazil
S. Ahuja[a], C.A. Bernardes[a], L. Calligaris[a], T.R. Fernandez Perez Tomei[a], E.M. Gregores[b], P.G. Mercadante[b], S.F. Novaes[a], SandraS. Padula[a]

Institute for Nuclear Research and Nuclear Energy, Bulgarian Academy of Sciences, Sofia, Bulgaria
A. Aleksandrov, R. Hadjiiska, P. Iaydjiev, A. Marinov, M. Misheva, M. Rodozov, M. Shopova, G. Sultanov

University of Sofia, Sofia, Bulgaria
A. Dimitrov, L. Litov, B. Pavlov, P. Petkov

Beihang University, Beijing, China
W. Fang[5], X. Gao[5], L. Yuan

Institute of High Energy Physics, Beijing, China
M. Ahmad, J.G. Bian, G.M. Chen, H.S. Chen, M. Chen, Y. Chen, C.H. Jiang, D. Leggat, H. Liao, Z. Liu, S.M. Shaheen[6], A. Spiezia, J. Tao, E. Yazgan, H. Zhang, S. Zhang[6], J. Zhao

State Key Laboratory of Nuclear Physics and Technology, Peking University, Beijing, China
Y. Ban, G. Chen, A. Levin, J. Li, L. Li, Q. Li, Y. Mao, S.J. Qian, D. Wang

Tsinghua University, Beijing, China
Y. Wang

Universidad de Los Andes, Bogota, Colombia
C. Avila, A. Cabrera, C.A. Carrillo Montoya, L.F. Chaparro Sierra, C. Florez, C.F. González Hernández, M.A. Segura Delgado

University of Split, Faculty of Electrical Engineering, Mechanical Engineering and Naval Architecture, Split, Croatia
B. Courbon, N. Godinovic, D. Lelas, I. Puljak, T. Sculac

University of Split, Faculty of Science, Split, Croatia
Z. Antunovic, M. Kovac

Institute Rudjer Boskovic, Zagreb, Croatia
V. Brigljevic, D. Ferencek, K. Kadija, B. Mesic, M. Roguljic, A. Starodumov[7], T. Susa

University of Cyprus, Nicosia, Cyprus
M.W. Ather, A. Attikis, M. Kolosova, G. Mavromanolakis, J. Mousa, C. Nicolaou, F. Ptochos, P.A. Razis, H. Rykaczewski

Charles University, Prague, Czech Republic
M. Finger[8], M. Finger Jr.[8]

Escuela Politecnica Nacional, Quito, Ecuador
E. Ayala

Universidad San Francisco de Quito, Quito, Ecuador
E. Carrera Jarrin

Academy of Scientific Research and Technology of the Arab Republic of Egypt, Egyptian Network of High Energy Physics, Cairo, Egypt
A.A. Abdelalim[9,10], Y. Assran[11,12], A. Mohamed[10]

National Institute of Chemical Physics and Biophysics, Tallinn, Estonia
S. Bhowmik, A. Carvalho Antunes De Oliveira, R.K. Dewanjee, K. Ehataht, M. Kadastik, M. Raidal, C. Veelken

Department of Physics, University of Helsinki, Helsinki, Finland
P. Eerola, H. Kirschenmann, J. Pekkanen, M. Voutilainen

Helsinki Institute of Physics, Helsinki, Finland
J. Havukainen, J.K. Heikkilä, T. Järvinen, V. Karimäki, R. Kinnunen, T. Lampén, K. Lassila-Perini, S. Laurila, S. Lehti, T. Lindén, P. Luukka, T. Mäenpää, H. Siikonen, E. Tuominen, J. Tuominiemi

Lappeenranta University of Technology, Lappeenranta, Finland
T. Tuuva

IRFU, CEA, Université Paris-Saclay, Gif-sur-Yvette, France
M. Besancon, F. Couderc, M. Dejardin, D. Denegri, J.L. Faure, F. Ferri, S. Ganjour, A. Givernaud, P. Gras, G. Hamel de Monchenault, P. Jarry, C. Leloup, E. Locci, J. Malcles, G. Negro, J. Rander, A. Rosowsky, M.Ö. Sahin, M. Titov

Laboratoire Leprince-Ringuet, Ecole polytechnique, CNRS/IN2P3, Université Paris-Saclay, Palaiseau, France
A. Abdulsalam[13], C. Amendola, I. Antropov, F. Beaudette, P. Busson, C. Charlot, R. Granier de Cassagnac, I. Kucher, A. Lobanov, J. Martin Blanco, C. Martin Perez, M. Nguyen, C. Ochando, G. Ortona, P. Paganini, J. Rembser, R. Salerno, J.B. Sauvan, Y. Sirois, A.G. Stahl Leiton, A. Zabi, A. Zghiche

Université de Strasbourg, CNRS, IPHC UMR 7178, Strasbourg, France
J.-L. Agram[14], J. Andrea, D. Bloch, G. Bourgatte, J.-M. Brom, E.C. Chabert, V. Cherepanov, C. Collard, E. Conte[14], J.-C. Fontaine[14], D. Gelé, U. Goerlach, M. Jansová, A.-C. Le Bihan, N. Tonon, P. Van Hove

Centre de Calcul de l'Institut National de Physique Nucleaire et de Physique des Particules, CNRS/IN2P3, Villeurbanne, France
S. Gadrat

Université de Lyon, Université Claude Bernard Lyon 1, CNRS-IN2P3, Institut de Physique Nucléaire de Lyon, Villeurbanne, France
S. Beauceron, C. Bernet, G. Boudoul, N. Chanon, R. Chierici, D. Contardo, P. Depasse, H. El Mamouni, J. Fay, L. Finco, S. Gascon, M. Gouzevitch, G. Grenier, B. Ille, F. Lagarde, I.B. Laktineh, H. Lattaud, M. Lethuillier, L. Mirabito, S. Perries, A. Popov[15], V. Sordini, G. Touquet, M. Vander Donckt, S. Viret

Georgian Technical University, Tbilisi, Georgia
A. Khvedelidze[8]

Tbilisi State University, Tbilisi, Georgia
Z. Tsamalaidze[8]

RWTH Aachen University, I. Physikalisches Institut, Aachen, Germany
C. Autermann, L. Feld, M.K. Kiesel, K. Klein, M. Lipinski, M. Preuten, M.P. Rauch, C. Schomakers, J. Schulz, M. Teroerde, B. Wittmer

RWTH Aachen University, III. Physikalisches Institut A, Aachen, Germany
A. Albert, M. Erdmann, S. Erdweg, T. Esch, R. Fischer, S. Ghosh, T. Hebbeker, C. Heidemann, K. Hoepfner, H. Keller, L. Mastrolorenzo, M. Merschmeyer, A. Meyer, P. Millet, S. Mukherjee, T. Pook, A. Pozdnyakov, M. Radziej, H. Reithler, M. Rieger, A. Schmidt, D. Teyssier, S. Thüer

RWTH Aachen University, III. Physikalisches Institut B, Aachen, Germany
G. Flügge, O. Hlushchenko, T. Kress, T. Müller, A. Nehrkorn, A. Nowack, C. Pistone, O. Pooth, D. Roy, H. Sert, A. Stahl[16]

Deutsches Elektronen-Synchrotron, Hamburg, Germany
M. Aldaya Martin, T. Arndt, C. Asawatangtrakuldee, I. Babounikau, K. Beernaert, O. Behnke, U. Behrens, A. Bermúdez Martínez, D. Bertsche, A.A. Bin Anuar, K. Borras[17], V. Botta, A. Campbell, P. Connor, C. Contreras-Campana, V. Danilov, A. De Wit, M.M. Defranchis, C. Diez Pardos, D. Domínguez Damiani, G. Eckerlin, T. Eichhorn, A. Elwood, E. Eren, E. Gallo[18], A. Geiser, J.M. Grados Luyando, A. Grohsjean, M. Guthoff, M. Haranko, A. Harb, H. Jung, M. Kasemann, J. Keaveney, C. Kleinwort, J. Knolle, D. Krücker, W. Lange, T. Lenz, J. Leonard, K. Lipka, W. Lohmann[19], R. Mankel, I.-A. Melzer-Pellmann, A.B. Meyer, M. Meyer, M. Missiroli, G. Mittag, J. Mnich, V. Myronenko, S.K. Pflitsch, D. Pitzl, A. Raspereza, A. Saibel, M. Savitskyi, P. Saxena, P. Schütze, C. Schwanenberger, R. Shevchenko, A. Singh, H. Tholen, O. Turkot, A. Vagnerini, M. Van De Klundert, G.P. Van Onsem, R. Walsh, Y. Wen, K. Wichmann, C. Wissing, O. Zenaiev

University of Hamburg, Hamburg, Germany
R. Aggleton, S. Bein, L. Benato, A. Benecke, T. Dreyer, A. Ebrahimi, E. Garutti, D. Gonzalez, P. Gunnellini, J. Haller, A. Hinzmann, A. Karavdina, G. Kasieczka, R. Klanner, R. Kogler, N. Kovalchuk, S. Kurz, V. Kutzner, J. Lange, D. Marconi, J. Multhaup, M. Niedziela, C.E.N. Niemeyer, D. Nowatschin, A. Perieanu, A. Reimers, O. Rieger, C. Scharf, P. Schleper, S. Schumann, J. Schwandt, J. Sonneveld, H. Stadie, G. Steinbrück, F.M. Stober, M. Stöver, B. Vormwald, I. Zoi

Karlsruher Institut fuer Technologie, Karlsruhe, Germany
M. Akbiyik, C. Barth, M. Baselga, S. Baur, E. Butz, R. Caspart, T. Chwalek, F. Colombo, W. De Boer, A. Dierlamm, K. El Morabit, N. Faltermann, B. Freund, M. Giffels, M.A. Harrendorf, F. Hartmann[16], S.M. Heindl, U. Husemann, I. Katkov[15], S. Kudella, S. Mitra, M.U. Mozer, Th. Müller, M. Musich, M. Plagge, G. Quast, K. Rabbertz, M. Schröder, I. Shvetsov, H.J. Simonis, R. Ulrich, S. Wayand, M. Weber, T. Weiler, C. Wöhrmann, R. Wolf

Institute of Nuclear and Particle Physics (INPP), NCSR Demokritos, Aghia Paraskevi, Greece
G. Anagnostou, G. Daskalakis, T. Geralis, A. Kyriakis, D. Loukas, G. Paspalaki

National and Kapodistrian University of Athens, Athens, Greece
A. Agapitos, G. Karathanasis, P. Kontaxakis, A. Panagiotou, I. Papavergou, N. Saoulidou, K. Vellidis

National Technical University of Athens, Athens, Greece
K. Kousouris, I. Papakrivopoulos, G. Tsipolitis

University of Ioánnina, Ioánnina, Greece
I. Evangelou, C. Foudas, P. Gianneios, P. Katsoulis, P. Kokkas, S. Mallios, N. Manthos, I. Papadopoulos, E. Paradas, J. Strologas, F.A. Triantis, D. Tsitsonis

MTA-ELTE Lendület CMS Particle and Nuclear Physics Group, Eötvös Loránd University, Budapest, Hungary
M. Bartók[20], M. Csanad, N. Filipovic, P. Major, M.I. Nagy, G. Pasztor, O. Surányi, G.I. Veres

Wigner Research Centre for Physics, Budapest, Hungary
G. Bencze, C. Hajdu, D. Horvath[21], Á. Hunyadi, F. Sikler, T.Á. Vámi, V. Veszpremi, G. Vesztergombi†

Institute of Nuclear Research ATOMKI, Debrecen, Hungary
N. Beni, S. Czellar, J. Karancsi[20], A. Makovec, J. Molnar, Z. Szillasi

Institute of Physics, University of Debrecen, Debrecen, Hungary
P. Raics, Z.L. Trocsanyi, B. Ujvari

Indian Institute of Science (IISc), Bangalore, India
S. Choudhury, J.R. Komaragiri, P.C. Tiwari

National Institute of Science Education and Research, HBNI, Bhubaneswar, India
S. Bahinipati[23], C. Kar, P. Mal, K. Mandal, A. Nayak[24], S. Roy Chowdhury, D.K. Sahoo[23], S.K. Swain

Panjab University, Chandigarh, India
S. Bansal, S.B. Beri, V. Bhatnagar, S. Chauhan, R. Chawla, N. Dhingra, R. Gupta, A. Kaur, M. Kaur, S. Kaur, P. Kumari, M. Lohan, M. Meena, A. Mehta, K. Sandeep, S. Sharma, J.B. Singh, A.K. Virdi, G. Walia

University of Delhi, Delhi, India
A. Bhardwaj, B.C. Choudhary, R.B. Garg, M. Gola, S. Keshri, Ashok Kumar, S. Malhotra, M. Naimuddin, P. Priyanka, K. Ranjan, Aashaq Shah, R. Sharma

Saha Institute of Nuclear Physics, HBNI, Kolkata, India
R. Bhardwaj[25], M. Bharti[25], R. Bhattacharya, S. Bhattacharya, U. Bhawandeep[25], D. Bhowmik, S. Dey, S. Dutt[25], S. Dutta, S. Ghosh, M. Maity[26], K. Mondal, S. Nandan, A. Purohit, P.K. Rout, A. Roy, G. Saha, S. Sarkar, T. Sarkar[26], M. Sharan, B. Singh[25], S. Thakur[25]

Indian Institute of Technology Madras, Madras, India
P.K. Behera, A. Muhammad

Bhabha Atomic Research Centre, Mumbai, India
R. Chudasama, D. Dutta, V. Jha, V. Kumar, D.K. Mishra, P.K. Netrakanti, L.M. Pant, P. Shukla, P. Suggisetti

Tata Institute of Fundamental Research-A, Mumbai, India
T. Aziz, M.A. Bhat, S. Dugad, G.B. Mohanty, N. Sur, RavindraKumar Verma

Tata Institute of Fundamental Research-B, Mumbai, India
S. Banerjee, S. Bhattacharya, S. Chatterjee, P. Das, M. Guchait, Sa. Jain, S. Karmakar, S. Kumar, G. Majumder, K. Mazumdar, N. Sahoo

Indian Institute of Science Education and Research (IISER), Pune, India
S. Chauhan, S. Dube, V. Hegde, A. Kapoor, K. Kothekar, S. Pandey, A. Rane, A. Rastogi, S. Sharma

Institute for Research in Fundamental Sciences (IPM), Tehran, Iran
S. Chenarani[27], E. Eskandari Tadavani, S.M. Etesami[27], M. Khakzad, M. Mohammadi Najafabadi, M. Naseri, F. Rezaei Hosseinabadi, B. Safarzadeh[28], M. Zeinali

University College Dublin, Dublin, Ireland
M. Felcini, M. Grunewald

INFN Sezione di Bari [a], Università di Bari [b], Politecnico di Bari [c], Bari, Italy
M. Abbrescia[a,b], C. Calabria[a,b], A. Colaleo[a], D. Creanza[a,c], L. Cristella[a,b], N. De Filippis[a,c], M. De Palma[a,b], A. Di Florio[a,b], F. Errico[a,b], L. Fiore[a], A. Gelmi[a,b], G. Iaselli[a,c], M. Ince[a,b], S. Lezki[a,b], G. Maggi[a,c], M. Maggi[a], G. Miniello[a,b], S. My[a,b], S. Nuzzo[a,b], A. Pompili[a,b], G. Pugliese[a,c], R. Radogna[a], A. Ranieri[a], G. Selvaggi[a,b], A. Sharma[a], L. Silvestris[a], R. Venditti[a], P. Verwilligen[a]

INFN Sezione di Bologna [a], Università di Bologna [b], Bologna, Italy
G. Abbiendi[a], C. Battilana[a,b], D. Bonacorsi[a,b], L. Borgonovi[a,b], S. Braibant-Giacomelli[a,b], R. Campanini[a,b], P. Capiluppi[a,b], A. Castro[a,b], F.R. Cavallo[a], S.S. Chhibra[a,b], G. Codispoti[a,b], M. Cuffiani[a,b], G.M. Dallavalle[a], F. Fabbri[a], A. Fanfani[a,b], E. Fontanesi, P. Giacomelli[a], C. Grandi[a], L. Guiducci[a,b], F. Iemmi[a,b], S. Lo Meo[a,29], S. Marcellini[a], G. Masetti[a], A. Montanari[a], F.L. Navarria[a,b], A. Perrotta[a], F. Primavera[a,b], A.M. Rossi[a,b], T. Rovelli[a,b], G.P. Siroli[a,b], N. Tosi[a]

INFN Sezione di Catania [a], Università di Catania [b], Catania, Italy
S. Albergo[a,b], A. Di Mattia[a], R. Potenza[a,b], A. Tricomi[a,b], C. Tuve[a,b]

INFN Sezione di Firenze [a], Università di Firenze [b], Firenze, Italy
G. Barbagli[a], K. Chatterjee[a,b], V. Ciulli[a,b], C. Civinini[a], R. D'Alessandro[a,b], E. Focardi[a,b], G. Latino, P. Lenzi[a,b], M. Meschini[a], S. Paoletti[a], L. Russo[a,30], G. Sguazzoni[a], D. Strom[a], L. Viliani[a]

INFN Laboratori Nazionali di Frascati, Frascati, Italy
L. Benussi, S. Bianco, F. Fabbri, D. Piccolo

INFN Sezione di Genova [a], Università di Genova [b], Genova, Italy
F. Ferro[a], R. Mulargia[a,b], E. Robutti[a], S. Tosi[a,b]

INFN Sezione di Milano-Bicocca [a], Università di Milano-Bicocca [b], Milano, Italy
A. Benaglia[a], A. Beschi[b], F. Brivio[a,b], V. Ciriolo[a,b,16], S. Di Guida[a,b,16], M.E. Dinardo[a,b], S. Fiorendi[a,b], S. Gennai[a], A. Ghezzi[a,b], P. Govoni[a,b], M. Malberti[a,b], S. Malvezzi[a], D. Menasce[a], F. Monti, L. Moroni[a], M. Paganoni[a,b], D. Pedrini[a], S. Ragazzi[a,b], T. Tabarelli de Fatis[a,b], D. Zuolo[a,b]

INFN Sezione di Napoli [a], Università di Napoli 'Federico II' [b], Napoli, Italy, Università della Basilicata [c], Potenza, Italy, Università G. Marconi [d], Roma, Italy
S. Buontempo[a], N. Cavallo[a,c], A. De Iorio[a,b], A. Di Crescenzo[a,b], F. Fabozzi[a,c], F. Fienga[a], G. Galati[a], A.O.M. Iorio[a,b], L. Lista[a], S. Meola[a,d,16], P. Paolucci[a,16], C. Sciacca[a,b], E. Voevodina[a,b]

INFN Sezione di Padova [a], Università di Padova [b], Padova, Italy, Università di Trento [c], Trento, Italy
P. Azzi[a], N. Bacchetta[a], D. Bisello[a,b], A. Boletti[a,b], A. Bragagnolo, R. Carlin[a,b], P. Checchia[a], M. Dall'Osso[a,b], P. De Castro Manzano[a], T. Dorigo[a], U. Dosselli[a], F. Gasparini[a,b], U. Gasparini[a,b], A. Gozzelino[a], S.Y. Hoh, S. Lacaprara[a], P. Lujan, M. Margoni[a,b], A.T. Meneguzzo[a,b], J. Pazzini[a,b], M. Presilla[b], P. Ronchese[a,b], R. Rossin[a,b], F. Simonetto[a,b], A. Tiko, E. Torassa[a], M. Tosi[a,b], M. Zanetti[a,b], P. Zotto[a,b], G. Zumerle[a,b]

INFN Sezione di Pavia [a], Università di Pavia [b], Pavia, Italy
A. Braghieri[a], A. Magnani[a], P. Montagna[a,b], S.P. Ratti[a,b], V. Re[a], M. Ressegotti[a,b], C. Riccardi[a,b], P. Salvini[a], I. Vai[a,b], P. Vitulo[a,b]

INFN Sezione di Perugia [a], Università di Perugia [b], Perugia, Italy
M. Biasini[a,b], G.M. Bilei[a], C. Cecchi[a,b], D. Ciangottini[a,b], L. Fanò[a,b], P. Lariccia[a,b], R. Leonardi[a,b], E. Manoni[a], G. Mantovani[a,b], V. Mariani[a,b], M. Menichelli[a], A. Rossi[a,b], A. Santocchia[a,b], D. Spiga[a]

INFN Sezione di Pisa [a], Università di Pisa [b], Scuola Normale Superiore di Pisa [c], Pisa, Italy
K. Androsov[a], P. Azzurri[a], G. Bagliesi[a], L. Bianchini[a], T. Boccali[a], L. Borrello, R. Castaldi[a], M.A. Ciocci[a,b], R. Dell'Orso[a], G. Fedi[a], F. Fiori[a,c], L. Giannini[a,c], A. Giassi[a], M.T. Grippo[a], F. Ligabue[a,c], E. Manca[a,c], G. Mandorli[a,c], A. Messineo[a,b], F. Palla[a], A. Rizzi[a,b], G. Rolandi[31], P. Spagnolo[a], R. Tenchini[a], G. Tonelli[a,b], A. Venturi[a], P.G. Verdini[a]

INFN Sezione di Roma [a], Sapienza Università di Roma [b], Rome, Italy
L. Barone[a,b], F. Cavallari[a], M. Cipriani[a,b], D. Del Re[a,b], E. Di Marco[a,b], M. Diemoz[a], S. Gelli[a,b], E. Longo[a,b], B. Marzocchi[a,b], P. Meridiani[a], G. Organtini[a,b], F. Pandolfi[a], R. Paramatti[a,b], F. Preiato[a,b], S. Rahatlou[a,b], C. Rovelli[a], F. Santanastasio[a,b]

INFN Sezione di Torino [a], Università di Torino [b], Torino, Italy, Università del Piemonte Orientale [c], Novara, Italy
N. Amapane[a,b], R. Arcidiacono[a,c], S. Argiro[a,b], M. Arneodo[a,c], N. Bartosik[a], R. Bellan[a,b], C. Biino[a], A. Cappati[a,b], N. Cartiglia[a], F. Cenna[a,b], S. Cometti[a], M. Costa[a,b], R. Covarelli[a,b], N. Demaria[a], B. Kiani[a,b], C. Mariotti[a], S. Maselli[a], E. Migliore[a,b], V. Monaco[a,b], E. Monteil[a,b], M. Monteno[a], M.M. Obertino[a,b], L. Pacher[a,b], N. Pastrone[a], M. Pelliccioni[a], G.L. Pinna Angioni[a,b], A. Romero[a,b], M. Ruspa[a,c], R. Sacchi[a,b], R. Salvatico[a,b], K. Shchelina[a,b], V. Sola[a], A. Solano[a,b], D. Soldi[a,b], A. Staiano[a]

INFN Sezione di Trieste [a], Università di Trieste [b], Trieste, Italy
S. Belforte[a], V. Candelise[a,b], M. Casarsa[a], F. Cossutti[a], A. Da Rold[a,b], G. Della Ricca[a,b], F. Vazzoler[a,b], A. Zanetti[a]

Kyungpook National University, Daegu, Korea
D.H. Kim, G.N. Kim, M.S. Kim, J. Lee, S. Lee, S.W. Lee, C.S. Moon, Y.D. Oh, S.I. Pak, S. Sekmen, D.C. Son, Y.C. Yang

Chonnam National University, Institute for Universe and Elementary Particles, Kwangju, Korea
H. Kim, D.H. Moon, G. Oh

Hanyang University, Seoul, Korea
B. Francois, J. Goh[32], T.J. Kim

Korea University, Seoul, Korea
S. Cho, S. Choi, Y. Go, D. Gyun, S. Ha, B. Hong, Y. Jo, K. Lee, K.S. Lee, S. Lee, J. Lim, S.K. Park, Y. Roh

Sejong University, Seoul, Korea
H.S. Kim

Seoul National University, Seoul, Korea
J. Almond, J. Kim, J.S. Kim, H. Lee, K. Lee, K. Nam, S.B. Oh, B.C. Radburn-Smith, S.h. Seo, U.K. Yang, H.D. Yoo, G.B. Yu

University of Seoul, Seoul, Korea
D. Jeon, H. Kim, J.H. Kim, J.S.H. Lee, I.C. Park

Sungkyunkwan University, Suwon, Korea
Y. Choi, C. Hwang, J. Lee, I. Yu

Riga Technical University, Riga, Latvia
V. Veckalns[33]

Vilnius University, Vilnius, Lithuania
V. Dudenas, A. Juodagalvis, J. Vaitkus

National Centre for Particle Physics, Universiti Malaya, Kuala Lumpur, Malaysia
Z.A. Ibrahim, M.A.B. Md Ali[34], F. Mohamad Idris[35], W.A.T. Wan Abdullah, M.N. Yusli, Z. Zolkapli

Universidad de Sonora (UNISON), Hermosillo, Mexico
J.F. Benitez, A. Castaneda Hernandez, J.A. Murillo Quijada

Centro de Investigacion y de Estudios Avanzados del IPN, Mexico City, Mexico
H. Castilla-Valdez, E. De La Cruz-Burelo, M.C. Duran-Osuna, I. Heredia-De La Cruz[36], R. Lopez-Fernandez, J. Mejia Guisao, R.I. Rabadan-Trejo, M. Ramirez-Garcia, G. Ramirez-Sanchez, R. Reyes-Almanza, A. Sanchez-Hernandez

Universidad Iberoamericana, Mexico City, Mexico
S. Carrillo Moreno, C. Oropeza Barrera, F. Vazquez Valencia

Benemerita Universidad Autonoma de Puebla, Puebla, Mexico
J. Eysermans, I. Pedraza, H.A. Salazar Ibarguen, C. Uribe Estrada

Universidad Autónoma de San Luis Potosí, San Luis Potosí, Mexico
A. Morelos Pineda

University of Auckland, Auckland, New Zealand
D. Krofcheck

University of Canterbury, Christchurch, New Zealand
S. Bheesette, P.H. Butler

National Centre for Physics, Quaid-I-Azam University, Islamabad, Pakistan
A. Ahmad, M. Ahmad, M.I. Asghar, Q. Hassan, H.R. Hoorani, W.A. Khan, M.A. Shah, M. Shoaib, M. Waqas

National Centre for Nuclear Research, Swierk, Poland
H. Bialkowska, M. Bluj, B. Boimska, T. Frueboes, M. Górski, M. Kazana, M. Szleper, P. Traczyk, P. Zalewski

Institute of Experimental Physics, Faculty of Physics, University of Warsaw, Warsaw, Poland
K. Bunkowski, A. Byszuk[37], K. Doroba, A. Kalinowski, M. Konecki, J. Krolikowski, M. Misiura, M. Olszewski, A. Pyskir, M. Walczak

Laboratório de Instrumentação e Física Experimental de Partículas, Lisboa, Portugal
M. Araujo, P. Bargassa, C. Beirão Da Cruz E Silva, A. Di Francesco, P. Faccioli, B. Galinhas, M. Gallinaro, J. Hollar, N. Leonardo, J. Seixas, G. Strong, O. Toldaiev, J. Varela

Joint Institute for Nuclear Research, Dubna, Russia
S. Afanasiev, P. Bunin, M. Gavrilenko, I. Golutvin, I. Gorbunov, A. Kamenev, V. Karjavine, A. Lanev, A. Malakhov, V. Matveev[38,39], P. Moisenz, V. Palichik, V. Perelygin, S. Shmatov, S. Shulha, N. Skatchkov, V. Smirnov, N. Voytishin, A. Zarubin

Petersburg Nuclear Physics Institute, Gatchina (St. Petersburg), Russia
V. Golovtsov, Y. Ivanov, V. Kim[40], E. Kuznetsova[41], P. Levchenko, V. Murzin, V. Oreshkin, I. Smirnov, D. Sosnov, V. Sulimov, L. Uvarov, S. Vavilov, A. Vorobyev

Institute for Nuclear Research, Moscow, Russia
Yu. Andreev, A. Dermenev, S. Gninenko, N. Golubev, A. Karneyeu, M. Kirsanov, N. Krasnikov, A. Pashenkov, A. Shabanov, D. Tlisov, A. Toropin

Institute for Theoretical and Experimental Physics, Moscow, Russia
V. Epshteyn, V. Gavrilov, N. Lychkovskaya, V. Popov, I. Pozdnyakov, G. Safronov, A. Spiridonov, A. Stepennov, V. Stolin, M. Toms, E. Vlasov, A. Zhokin

Moscow Institute of Physics and Technology, Moscow, Russia
T. Aushev

National Research Nuclear University 'Moscow Engineering Physics Institute' (MEPhI), Moscow, Russia
R. Chistov[42], M. Danilov[42], S. Polikarpov[42], E. Tarkovskii

P.N. Lebedev Physical Institute, Moscow, Russia
V. Andreev, M. Azarkin, I. Dremin[39], M. Kirakosyan, A. Terkulov

Skobeltsyn Institute of Nuclear Physics, Lomonosov Moscow State University, Moscow, Russia
A. Baskakov, A. Belyaev, E. Boos, V. Bunichev, M. Dubinin[43], L. Dudko, A. Gribushin, V. Klyukhin, O. Kodolova, I. Lokhtin, S. Obraztsov, S. Petrushanko, V. Savrin

Novosibirsk State University (NSU), Novosibirsk, Russia
A. Barnyakov[44], V. Blinov[44], T. Dimova[44], L. Kardapoltsev[44], Y. Skovpen[44]

Institute for High Energy Physics of National Research Centre 'Kurchatov Institute', Protvino, Russia
I. Azhgirey, I. Bayshev, S. Bitioukov, V. Kachanov, A. Kalinin, D. Konstantinov, P. Mandrik, V. Petrov, R. Ryutin, S. Slabospitskii, A. Sobol, S. Troshin, N. Tyurin, A. Uzunian, A. Volkov

National Research Tomsk Polytechnic University, Tomsk, Russia
A. Babaev, S. Baidali, V. Okhotnikov

University of Belgrade, Faculty of Physics and Vinca Institute of Nuclear Sciences, Belgrade, Serbia
P. Adzic[45], P. Cirkovic, D. Devetak, M. Dordevic, P. Milenovic[46], J. Milosevic

Centro de Investigaciones Energéticas Medioambientales y Tecnológicas (CIEMAT), Madrid, Spain
J. Alcaraz Maestre, A. Álvarez Fernández, I. Bachiller, M. Barrio Luna, J.A. Brochero Cifuentes, M. Cerrada, N. Colino, B. De La Cruz, A. Delgado Peris, C. Fernandez Bedoya, J.P. Fernández Ramos, J. Flix, M.C. Fouz, O. Gonzalez Lopez, S. Goy Lopez, J.M. Hernandez, M.I. Josa, D. Moran, A. Pérez-Calero Yzquierdo, J. Puerta Pelayo, I. Redondo, L. Romero, S. Sánchez Navas, M.S. Soares, A. Triossi

Universidad Autónoma de Madrid, Madrid, Spain
C. Albajar, J.F. de Trocóniz

Universidad de Oviedo, Oviedo, Spain
J. Cuevas, C. Erice, J. Fernandez Menendez, S. Folgueras, I. Gonzalez Caballero, J.R. González Fernández, E. Palencia Cortezon, V. Rodríguez Bouza, S. Sanchez Cruz, J.M. Vizan Garcia

Instituto de Física de Cantabria (IFCA), CSIC-Universidad de Cantabria, Santander, Spain
I.J. Cabrillo, A. Calderon, B. Chazin Quero, J. Duarte Campderros, M. Fernandez, P.J. Fernández Manteca, A. García Alonso, J. Garcia-Ferrero, G. Gomez, A. Lopez Virto, J. Marco, C. Martinez Rivero, P. Martinez Ruiz del Arbol, F. Matorras, J. Piedra Gomez, C. Prieels, T. Rodrigo, A. Ruiz-Jimeno, L. Scodellaro, N. Trevisani, I. Vila, R. Vilar Cortabitarte

University of Ruhuna, Department of Physics, Matara, Sri Lanka
N. Wickramage

CERN, European Organization for Nuclear Research, Geneva, Switzerland
D. Abbaneo, B. Akgun, E. Auffray, G. Auzinger, P. Baillon, A.H. Ball, D. Barney, J. Bendavid, M. Bianco, A. Bocci, C. Botta, E. Brondolin, T. Camporesi, M. Cepeda, G. Cerminara, E. Chapon, Y. Chen, G. Cucciati, D. d'Enterria, A. Dabrowski, N. Daci, V. Daponte, A. David, A. De Roeck, N. Deelen, M. Dobson, M. Dünser, N. Dupont, A. Elliott-Peisert, F. Fallavollita[47], D. Fasanella, G. Franzoni, J. Fulcher, W. Funk, D. Gigi, A. Gilbert, K. Gill, F. Glege, M. Gruchala, M. Guilbaud, D. Gulhan, J. Hegeman, C. Heidegger, V. Innocente, G.M. Innocenti, A. Jafari, P. Janot, O. Karacheban[19], J. Kieseler, A. Kornmayer, M. Krammer[1], C. Lange, P. Lecoq, C. Lourenço, L. Malgeri, M. Mannelli, A. Massironi, F. Meijers, J.A. Merlin, S. Mersi, E. Meschi, F. Moortgat, M. Mulders, J. Ngadiuba, S. Nourbakhsh, S. Orfanelli, L. Orsini, F. Pantaleo[16], L. Pape, E. Perez, M. Peruzzi, A. Petrilli, G. Petrucciani, A. Pfeiffer, M. Pierini, F.M. Pitters, D. Rabady, A. Racz, M. Rovere, H. Sakulin, C. Schäfer, C. Schwick, M. Selvaggi, A. Sharma, P. Silva, P. Sphicas[48], A. Stakia, J. Steggemann, D. Treille, A. Tsirou, A. Vartak, M. Verzetti, W.D. Zeuner

Paul Scherrer Institut, Villigen, Switzerland
L. Caminada[49], K. Deiters, W. Erdmann, R. Horisberger, Q. Ingram, H.C. Kaestli, D. Kotlinski, U. Langenegger, T. Rohe, S.A. Wiederkehr

ETH Zurich - Institute for Particle Physics and Astrophysics (IPA), Zurich, Switzerland
M. Backhaus, L. Bäni, P. Berger, N. Chernyavskaya, G. Dissertori, M. Dittmar, M. Donegà, C. Dorfer, T.A. Gómez Espinosa, C. Grab, D. Hits, T. Klijnsma, W. Lustermann, R.A. Manzoni, M. Marionneau, M.T. Meinhard, F. Micheli, P. Musella, F. Nessi-Tedaldi, F. Pauss, G. Perrin, L. Perrozzi, S. Pigazzini, M. Reichmann, C. Reissel, D. Ruini, D.A. Sanz Becerra, M. Schönenberger, L. Shchutska, V.R. Tavolaro, K. Theofilatos, M.L. Vesterbacka Olsson, R. Wallny, D.H. Zhu

Universität Zürich, Zurich, Switzerland
T.K. Aarrestad, C. Amsler[50], D. Brzhechko, M.F. Canelli, A. De Cosa, R. Del Burgo, S. Donato, C. Galloni, T. Hreus, B. Kilminster, S. Leontsinis, I. Neutelings, G. Rauco, P. Robmann, D. Salerno, K. Schweiger, C. Seitz, Y. Takahashi, S. Wertz, A. Zucchetta

National Central University, Chung-Li, Taiwan
T.H. Doan, R. Khurana, C.M. Kuo, W. Lin, S.S. Yu

National Taiwan University (NTU), Taipei, Taiwan
P. Chang, Y. Chao, K.F. Chen, P.H. Chen, W.-S. Hou, Y.F. Liu, R.-S. Lu, E. Paganis, A. Psallidas, A. Steen

Chulalongkorn University, Faculty of Science, Department of Physics, Bangkok, Thailand
B. Asavapibhop, N. Srimanobhas, N. Suwonjandee

Çukurova University, Physics Department, Science and Art Faculty, Adana, Turkey
A. Bat, F. Boran, S. Cerci[51], S. Damarseckin, Z.S. Demiroglu, F. Dolek, C. Dozen, I. Dumanoglu, G. Gokbulut, Y. Guler, E. Gurpinar, I. Hos[52], C. Isik, E.E. Kangal[53], O. Kara, A. Kayis Topaksu, U. Kiminsu, M. Oglakci, G. Onengut, K. Ozdemir[54], S. Ozturk[55], D. Sunar Cerci[51], B. Tali[51], U.G. Tok, S. Turkcapar, I.S. Zorbakir, C. Zorbilmez

Middle East Technical University, Physics Department, Ankara, Turkey
B. Isildak[56], G. Karapinar[57], M. Yalvac, M. Zeyrek

Bogazici University, Istanbul, Turkey
I.O. Atakisi, E. Gülmez, M. Kaya[58], O. Kaya[59], S. Ozkorucuklu[60], S. Tekten, E.A. Yetkin[61]

Istanbul Technical University, Istanbul, Turkey
M.N. Agaras, A. Cakir, K. Cankocak, Y. Komurcu, S. Sen[62]

Institute for Scintillation Materials of National Academy of Science of Ukraine, Kharkov, Ukraine
B. Grynyov

National Scientific Center, Kharkov Institute of Physics and Technology, Kharkov, Ukraine
L. Levchuk

University of Bristol, Bristol, United Kingdom
F. Ball, J.J. Brooke, D. Burns, E. Clement, D. Cussans, O. Davignon, H. Flacher, J. Goldstein, G.P. Heath, H.F. Heath, L. Kreczko, D.M. Newbold[63], S. Paramesvaran, B. Penning, T. Sakuma, D. Smith, V.J. Smith, J. Taylor, A. Titterton

Rutherford Appleton Laboratory, Didcot, United Kingdom
K.W. Bell, A. Belyaev[64], C. Brew, R.M. Brown, D. Cieri, D.J.A. Cockerill, J.A. Coughlan, K. Harder, S. Harper, J. Linacre, K. Manolopoulos, E. Olaiya, D. Petyt, T. Reis, T. Schuh, C.H. Shepherd-Themistocleous, A. Thea, I.R. Tomalin, T. Williams, W.J. Womersley

Imperial College, London, United Kingdom
R. Bainbridge, P. Bloch, J. Borg, S. Breeze, O. Buchmuller, A. Bundock, D. Colling, P. Dauncey, G. Davies, M. Della Negra, R. Di Maria, P. Everaerts, G. Hall, G. Iles, T. James, M. Komm, C. Laner, L. Lyons, A.-M. Magnan, S. Malik, A. Martelli, J. Nash[65], A. Nikitenko[7], V. Palladino, M. Pesaresi, D.M. Raymond, A. Richards, A. Rose, E. Scott, C. Seez, A. Shtipliyski, G. Singh, M. Stoye, T. Strebler, S. Summers, A. Tapper, K. Uchida, T. Virdee[16], N. Wardle, D. Winterbottom, J. Wright, S.C. Zenz

Brunel University, Uxbridge, United Kingdom
J.E. Cole, P.R. Hobson, A. Khan, P. Kyberd, C.K. Mackay, A. Morton, I.D. Reid, L. Teodorescu, S. Zahid

Baylor University, Waco, USA
K. Call, J. Dittmann, K. Hatakeyama, H. Liu, C. Madrid, B. McMaster, N. Pastika, C. Smith

Catholic University of America, Washington, DC, USA
R. Bartek, A. Dominguez

The University of Alabama, Tuscaloosa, USA
A. Buccilli, S.I. Cooper, C. Henderson, P. Rumerio, C. West

Boston University, Boston, USA
D. Arcaro, T. Bose, Z. Demiragli, D. Gastler, S. Girgis, D. Pinna, C. Richardson, J. Rohlf, D. Sperka, I. Suarez, L. Sulak, D. Zou

Brown University, Providence, USA
G. Benelli, B. Burkle, X. Coubez, D. Cutts, M. Hadley, J. Hakala, U. Heintz, J.M. Hogan[66], K.H.M. Kwok, E. Laird, G. Landsberg, J. Lee, Z. Mao, M. Narain, S. Sagir[67], R. Syarif, E. Usai, D. Yu

University of California, Davis, Davis, USA
R. Band, C. Brainerd, R. Breedon, D. Burns, M. Calderon De La Barca Sanchez, M. Chertok, J. Conway, R. Conway, P.T. Cox, R. Erbacher, C. Flores, G. Funk, W. Ko, O. Kukral, R. Lander, M. Mulhearn, D. Pellett, J. Pilot, S. Shalhout, M. Shi, D. Stolp, D. Taylor, K. Tos, M. Tripathi, Z. Wang, F. Zhang

University of California, Los Angeles, USA
M. Bachtis, C. Bravo, R. Cousins, A. Dasgupta, S. Erhan, A. Florent, J. Hauser, M. Ignatenko, N. Mccoll, S. Regnard, D. Saltzberg, C. Schnaible, V. Valuev

University of California, Riverside, Riverside, USA
E. Bouvier, K. Burt, R. Clare, J.W. Gary, S.M.A. Ghiasi Shirazi, G. Hanson, G. Karapostoli, E. Kennedy, F. Lacroix, O.R. Long, M. Olmedo Negrete, M.I. Paneva, W. Si, L. Wang, H. Wei, S. Wimpenny, B.R. Yates

University of California, San Diego, La Jolla, USA
J.G. Branson, P. Chang, S. Cittolin, M. Derdzinski, R. Gerosa, D. Gilbert, B. Hashemi, A. Holzner, D. Klein, G. Kole, V. Krutelyov, J. Letts, M. Masciovecchio, S. May, D. Olivito, S. Padhi, M. Pieri, V. Sharma, M. Tadel, J. Wood, F. Würthwein, A. Yagil, G. Zevi Della Porta

University of California, Santa Barbara - Department of Physics, Santa Barbara, USA
N. Amin, R. Bhandari, C. Campagnari, M. Citron, V. Dutta, M. Franco Sevilla, L. Gouskos, R. Heller, J. Incandela, H. Mei, A. Ovcharova, H. Qu, J. Richman, D. Stuart, S. Wang, J. Yoo

California Institute of Technology, Pasadena, USA
D. Anderson, A. Bornheim, J.M. Lawhorn, N. Lu, H.B. Newman, T.Q. Nguyen, J. Pata, M. Spiropulu, J.R. Vlimant, R. Wilkinson, S. Xie, Z. Zhang, R.Y. Zhu

Carnegie Mellon University, Pittsburgh, USA
M.B. Andrews, T. Ferguson, T. Mudholkar, M. Paulini, M. Sun, I. Vorobiev, M. Weinberg

University of Colorado Boulder, Boulder, USA
J.P. Cumalat, W.T. Ford, F. Jensen, A. Johnson, E. MacDonald, T. Mulholland, R. Patel, A. Perloff, K. Stenson, K.A. Ulmer, S.R. Wagner

Cornell University, Ithaca, USA
J. Alexander, J. Chaves, Y. Cheng, J. Chu, A. Datta, K. Mcdermott, N. Mirman, J.R. Patterson, D. Quach, A. Rinkevicius, A. Ryd, L. Skinnari, L. Soffi, S.M. Tan, Z. Tao, J. Thom, J. Tucker, P. Wittich, M. Zientek

Fermi National Accelerator Laboratory, Batavia, USA
S. Abdullin, M. Albrow, M. Alyari, G. Apollinari, A. Apresyan, A. Apyan, S. Banerjee, L.A.T. Bauerdick, A. Beretvas, J. Berryhill, P.C. Bhat, K. Burkett, J.N. Butler, A. Canepa, G.B. Cerati, H.W.K. Cheung, F. Chlebana, M. Cremonesi, J. Duarte, V.D. Elvira, J. Freeman, Z. Gecse, E. Gottschalk, L. Gray, D. Green, S. Grünendahl, O. Gutsche, J. Hanlon, R.M. Harris, S. Hasegawa, J. Hirschauer, Z. Hu, B. Jayatilaka, S. Jindariani, M. Johnson, U. Joshi, B. Klima, M.J. Kortelainen, B. Kreis, S. Lammel, D. Lincoln, R. Lipton, M. Liu, T. Liu, J. Lykken, K. Maeshima, J.M. Marraffino, D. Mason, P. McBride, P. Merkel, S. Mrenna, S. Nahn, V. O'Dell, K. Pedro, C. Pena, O. Prokofyev, G. Rakness, F. Ravera, A. Reinsvold, L. Ristori, A. Savoy-Navarro[68], B. Schneider, E. Sexton-Kennedy, A. Soha, W.J. Spalding, L. Spiegel, S. Stoynev, J. Strait, N. Strobbe, L. Taylor, S. Tkaczyk, N.V. Tran, L. Uplegger, E.W. Vaandering, C. Vernieri, M. Verzocchi, R. Vidal, M. Wang, H.A. Weber

University of Florida, Gainesville, USA
D. Acosta, P. Avery, P. Bortignon, D. Bourilkov, A. Brinkerhoff, L. Cadamuro, A. Carnes, D. Curry, R.D. Field, S.V. Gleyzer, B.M. Joshi, J. Konigsberg, A. Korytov, K.H. Lo, P. Ma, K. Matchev, N. Menendez, G. Mitselmakher, D. Rosenzweig, K. Shi, J. Wang, S. Wang, X. Zuo

Florida International University, Miami, USA
Y.R. Joshi, S. Linn

Florida State University, Tallahassee, USA
A. Ackert, T. Adams, A. Askew, S. Hagopian, V. Hagopian, K.F. Johnson, T. Kolberg, G. Martinez, T. Perry, H. Prosper, A. Saha, C. Schiber, R. Yohay

Florida Institute of Technology, Melbourne, USA
M.M. Baarmand, V. Bhopatkar, S. Colafranceschi, M. Hohlmann, D. Noonan, M. Rahmani, T. Roy, M. Saunders, F. Yumiceva

University of Illinois at Chicago (UIC), Chicago, USA
M.R. Adams, L. Apanasevich, D. Berry, R.R. Betts, R. Cavanaugh, X. Chen, S. Dittmer, O. Evdokimov, C.E. Gerber, D.A. Hangal, D.J. Hofman, K. Jung, J. Kamin, C. Mills, M.B. Tonjes, N. Varelas, H. Wang, X. Wang, Z. Wu, J. Zhang

The University of Iowa, Iowa City, USA
M. Alhusseini, B. Bilki[69], W. Clarida, K. Dilsiz[70], S. Durgut, R.P. Gandrajula, M. Haytmyradov, V. Khristenko, J.-P. Merlo, A. Mestvirishvili, A. Moeller, J. Nachtman, H. Ogul[71], Y. Onel, F. Ozok[72], A. Penzo, C. Snyder, E. Tiras, J. Wetzel

Johns Hopkins University, Baltimore, USA
B. Blumenfeld, A. Cocoros, N. Eminizer, D. Fehling, L. Feng, A.V. Gritsan, W.T. Hung, P. Maksimovic, J. Roskes, U. Sarica, M. Swartz, M. Xiao

The University of Kansas, Lawrence, USA
A. Al-bataineh, P. Baringer, A. Bean, S. Boren, J. Bowen, A. Bylinkin, J. Castle, S. Khalil, A. Kropivnitskaya, D. Majumder, W. Mcbrayer, M. Murray, C. Rogan, S. Sanders, E. Schmitz, J.D. Tapia Takaki, Q. Wang

Kansas State University, Manhattan, USA
S. Duric, A. Ivanov, K. Kaadze, D. Kim, Y. Maravin, D.R. Mendis, T. Mitchell, A. Modak, A. Mohammadi

Lawrence Livermore National Laboratory, Livermore, USA
F. Rebassoo, D. Wright

University of Maryland, College Park, USA
A. Baden, O. Baron, A. Belloni, S.C. Eno, Y. Feng, C. Ferraioli, N.J. Hadley, S. Jabeen, G.Y. Jeng, R.G. Kellogg, J. Kunkle, A.C. Mignerey, S. Nabili, F. Ricci-Tam, M. Seidel, Y.H. Shin, A. Skuja, S.C. Tonwar, K. Wong

Massachusetts Institute of Technology, Cambridge, USA
D. Abercrombie, B. Allen, V. Azzolini, A. Baty, R. Bi, S. Brandt, W. Busza, I.A. Cali, M. D'Alfonso, G. Gomez Ceballos, M. Goncharov, P. Harris, D. Hsu, M. Hu, Y. Iiyama, M. Klute, D. Kovalskyi, Y.-J. Lee, P.D. Luckey, B. Maier, A.C. Marini, C. Mcginn, C. Mironov, S. Narayanan, X. Niu, C. Paus, D. Rankin, C. Roland, G. Roland, Z. Shi, G.S.F. Stephans, K. Sumorok, K. Tatar, D. Velicanu, J. Wang, T.W. Wang, B. Wyslouch

University of Minnesota, Minneapolis, USA
A.C. Benvenuti[†], R.M. Chatterjee, A. Evans, P. Hansen, J. Hiltbrand, Sh. Jain, S. Kalafut, M. Krohn, Y. Kubota, Z. Lesko, J. Mans, R. Rusack, M.A. Wadud

University of Mississippi, Oxford, USA
J.G. Acosta, S. Oliveros

University of Nebraska-Lincoln, Lincoln, USA
E. Avdeeva, K. Bloom, D.R. Claes, C. Fangmeier, F. Golf, R. Gonzalez Suarez, R. Kamalieddin, I. Kravchenko, J. Monroy, J.E. Siado, G.R. Snow, B. Stieger

State University of New York at Buffalo, Buffalo, USA
A. Godshalk, C. Harrington, I. Iashvili, A. Kharchilava, C. Mclean, D. Nguyen, A. Parker, S. Rappoccio, B. Roozbahani

Northeastern University, Boston, USA
G. Alverson, E. Barberis, C. Freer, Y. Haddad, A. Hortiangtham, G. Madigan, D.M. Morse, T. Orimoto, A. Tishelman-charny, T. Wamorkar, B. Wang, A. Wisecarver, D. Wood

Northwestern University, Evanston, USA
S. Bhattacharya, J. Bueghly, O. Charaf, T. Gunter, K.A. Hahn, N. Odell, M.H. Schmitt, K. Sung, M. Trovato, M. Velasco

University of Notre Dame, Notre Dame, USA
R. Bucci, N. Dev, R. Goldouzian, M. Hildreth, K. Hurtado Anampa, C. Jessop, D.J. Karmgard, K. Lannon, W. Li, N. Loukas, N. Marinelli, F. Meng, C. Mueller, Y. Musienko[38], M. Planer, R. Ruchti, P. Siddireddy, G. Smith, S. Taroni, M. Wayne, A. Wightman, M. Wolf, A. Woodard

The Ohio State University, Columbus, USA
J. Alimena, L. Antonelli, B. Bylsma, L.S. Durkin, S. Flowers, B. Francis, C. Hill, W. Ji, T.Y. Ling, W. Luo, B.L. Winer

Princeton University, Princeton, USA
S. Cooperstein, G. Dezoort, P. Elmer, J. Hardenbrook, N. Haubrich, S. Higginbotham, A. Kalogeropoulos, S. Kwan, D. Lange, M.T. Lucchini, J. Luo, D. Marlow, K. Mei, I. Ojalvo, J. Olsen, C. Palmer, P. Piroué, J. Salfeld-Nebgen, D. Stickland, C. Tully

University of Puerto Rico, Mayaguez, USA
S. Malik, S. Norberg

Purdue University, West Lafayette, USA
A. Barker, V.E. Barnes, S. Das, L. Gutay, M. Jones, A.W. Jung, A. Khatiwada, B. Mahakud, D.H. Miller, N. Neumeister, C.C. Peng, S. Piperov, H. Qiu, J.F. Schulte, J. Sun, F. Wang, R. Xiao, W. Xie

Purdue University Northwest, Hammond, USA
T. Cheng, J. Dolen, N. Parashar

Rice University, Houston, USA
Z. Chen, K.M. Ecklund, S. Freed, F.J.M. Geurts, M. Kilpatrick, Arun Kumar, W. Li, B.P. Padley, R. Redjimi, J. Roberts, J. Rorie, W. Shi, Z. Tu, A. Zhang

University of Rochester, Rochester, USA
A. Bodek, P. de Barbaro, R. Demina, Y.t. Duh, J.L. Dulemba, C. Fallon, T. Ferbel, M. Galanti, A. Garcia-Bellido, J. Han, O. Hindrichs, A. Khukhunaishvili, E. Ranken, P. Tan, R. Taus

Rutgers, The State University of New Jersey, Piscataway, USA
B. Chiarito, J.P. Chou, Y. Gershtein, E. Halkiadakis, A. Hart, M. Heindl, E. Hughes, S. Kaplan, R. Kunnawalkam Elayavalli, S. Kyriacou, I. Laflotte, A. Lath, R. Montalvo, K. Nash, M. Osherson, H. Saka, S. Salur, S. Schnetzer, D. Sheffield, S. Somalwar, R. Stone, S. Thomas, P. Thomassen

University of Tennessee, Knoxville, USA
H. Acharya, A.G. Delannoy, J. Heideman, G. Riley, S. Spanier

Texas A&M University, College Station, USA
O. Bouhali[73], A. Celik, M. Dalchenko, M. De Mattia, A. Delgado, S. Dildick, R. Eusebi, J. Gilmore, T. Huang, T. Kamon[74], S. Luo, D. Marley, R. Mueller, D. Overton, L. Perniè, D. Rathjens, A. Safonov

Texas Tech University, Lubbock, USA
N. Akchurin, J. Damgov, F. De Guio, P.R. Dudero, S. Kunori, K. Lamichhane, S.W. Lee, T. Mengke, S. Muthumuni, T. Peltola, S. Undleeb, I. Volobouev, Z. Wang, A. Whitbeck

Vanderbilt University, Nashville, USA
S. Greene, A. Gurrola, R. Janjam, W. Johns, C. Maguire, A. Melo, H. Ni, K. Padeken, F. Romeo, P. Sheldon, S. Tuo, J. Velkovska, M. Verweij, Q. Xu

University of Virginia, Charlottesville, USA
M.W. Arenton, P. Barria, B. Cox, R. Hirosky, M. Joyce, A. Ledovskoy, H. Li, C. Neu, T. Sinthuprasith, Y. Wang, E. Wolfe, F. Xia

Wayne State University, Detroit, USA
R. Harr, P.E. Karchin, N. Poudyal, J. Sturdy, P. Thapa, S. Zaleski

University of Wisconsin - Madison, Madison, WI, USA
J. Buchanan, C. Caillol, D. Carlsmith, S. Dasu, I. De Bruyn, L. Dodd, B. Gomber[75], M. Grothe, M. Herndon, A. Hervé, U. Hussain, P. Klabbers, A. Lanaro, K. Long, R. Loveless, T. Ruggles, A. Savin, V. Sharma, N. Smith, W.H. Smith, N. Woods

†: Deceased
1: Also at Vienna University of Technology, Vienna, Austria
2: Also at IRFU, CEA, Université Paris-Saclay, Gif-sur-Yvette, France
3: Also at Universidade Estadual de Campinas, Campinas, Brazil
4: Also at Federal University of Rio Grande do Sul, Porto Alegre, Brazil
5: Also at Université Libre de Bruxelles, Bruxelles, Belgium
6: Also at University of Chinese Academy of Sciences, Beijing, China
7: Also at Institute for Theoretical and Experimental Physics, Moscow, Russia
8: Also at Joint Institute for Nuclear Research, Dubna, Russia
9: Also at Helwan University, Cairo, Egypt
10: Now at Zewail City of Science and Technology, Zewail, Egypt
11: Also at Suez University, Suez, Egypt
12: Now at British University in Egypt, Cairo, Egypt
13: Also at Department of Physics, King Abdulaziz University, Jeddah, Saudi Arabia
14: Also at Université de Haute Alsace, Mulhouse, France
15: Also at Skobeltsyn Institute of Nuclear Physics, Lomonosov Moscow State University, Moscow, Russia
16: Also at CERN, European Organization for Nuclear Research, Geneva, Switzerland
17: Also at RWTH Aachen University, III. Physikalisches Institut A, Aachen, Germany
18: Also at University of Hamburg, Hamburg, Germany
19: Also at Brandenburg University of Technology, Cottbus, Germany
20: Also at Institute of Physics, University of Debrecen, Debrecen, Hungary
21: Also at Institute of Nuclear Research ATOMKI, Debrecen, Hungary
22: Also at MTA-ELTE Lendület CMS Particle and Nuclear Physics Group, Eötvös Loránd University, Budapest, Hungary

23: Also at Indian Institute of Technology Bhubaneswar, Bhubaneswar, India
24: Also at Institute of Physics, Bhubaneswar, India
25: Also at Shoolini University, Solan, India
26: Also at University of Visva-Bharati, Santiniketan, India
27: Also at Isfahan University of Technology, Isfahan, Iran
28: Also at Plasma Physics Research Center, Science and Research Branch, Islamic Azad University, Tehran, Iran
29: Also at ITALIAN NATIONAL AGENCY FOR NEW TECHNOLOGIES, ENERGY AND SUSTAINABLE ECONOMIC DEVELOPMENT, Bologna, Italy
30: Also at Università degli Studi di Siena, Siena, Italy
31: Also at Scuola Normale e Sezione dell'INFN, Pisa, Italy
32: Also at Kyunghee University, Seoul, Korea
33: Also at Riga Technical University, Riga, Latvia
34: Also at International Islamic University of Malaysia, Kuala Lumpur, Malaysia
35: Also at Malaysian Nuclear Agency, MOSTI, Kajang, Malaysia
36: Also at Consejo Nacional de Ciencia y Tecnología, Mexico City, Mexico
37: Also at Warsaw University of Technology, Institute of Electronic Systems, Warsaw, Poland
38: Also at Institute for Nuclear Research, Moscow, Russia
39: Now at National Research Nuclear University 'Moscow Engineering Physics Institute' (MEPhI), Moscow, Russia
40: Also at St. Petersburg State Polytechnical University, St. Petersburg, Russia
41: Also at University of Florida, Gainesville, USA
42: Also at P.N. Lebedev Physical Institute, Moscow, Russia
43: Also at California Institute of Technology, Pasadena, USA
44: Also at Budker Institute of Nuclear Physics, Novosibirsk, Russia
45: Also at Faculty of Physics, University of Belgrade, Belgrade, Serbia
46: Also at University of Belgrade, Faculty of Physics and Vinca Institute of Nuclear Sciences, Belgrade, Serbia
47: Also at INFN Sezione di Pavia [a], Università di Pavia [b], Pavia, Italy
48: Also at National and Kapodistrian University of Athens, Athens, Greece
49: Also at Universität Zürich, Zurich, Switzerland
50: Also at Stefan Meyer Institute for Subatomic Physics (SMI), Vienna, Austria
51: Also at Adiyaman University, Adiyaman, Turkey
52: Also at Istanbul Aydin University, Istanbul, Turkey
53: Also at Mersin University, Mersin, Turkey
54: Also at Piri Reis University, Istanbul, Turkey
55: Also at Gaziosmanpasa University, Tokat, Turkey
56: Also at Ozyegin University, Istanbul, Turkey
57: Also at Izmir Institute of Technology, Izmir, Turkey
58: Also at Marmara University, Istanbul, Turkey
59: Also at Kafkas University, Kars, Turkey
60: Also at Istanbul University, Faculty of Science, Istanbul, Turkey
61: Also at Istanbul Bilgi University, Istanbul, Turkey
62: Also at Hacettepe University, Ankara, Turkey
63: Also at Rutherford Appleton Laboratory, Didcot, United Kingdom
64: Also at School of Physics and Astronomy, University of Southampton, Southampton, United Kingdom
65: Also at Monash University, Faculty of Science, Clayton, Australia
66: Also at Bethel University, St. Paul, USA

67: Also at Karamanoğlu Mehmetbey University, Karaman, Turkey
68: Also at Purdue University, West Lafayette, USA
69: Also at Beykent University, Istanbul, Turkey
70: Also at Bingol University, Bingol, Turkey
71: Also at Sinop University, Sinop, Turkey
72: Also at Mimar Sinan University, Istanbul, Istanbul, Turkey
73: Also at Texas A&M University at Qatar, Doha, Qatar
74: Also at Kyungpook National University, Daegu, Korea
75: Also at University of Hyderabad, Hyderabad, India